



Multi-targeting inulin-based nanoparticles with cannabidiol for effective prevention of ulcerative colitis

Xuan Zhang^{a,c,d}, Xia Gao^{a,c,d}, Xiangzhou Yi^{a,c,d}, Hui Yu^{a,c,d}, Mingyang Shao^{a,c,d},
Yongcheng Li^{a,c,d}, Xuanri Shen^{a,b,c,d,*}

^a College of Food Science and Engineering, Hainan University, Haikou, 570228, China

^b College of Food Science and Technology, Hainan Tropical Ocean University, Sanya, 572022, China

^c Key Laboratory of Food Nutrition and Functional Food of Hainan Province, Haikou, 570228, China

^d Hainan Engineering Research Center of Aquatic Resources Efficient Utilization in South China Sea, Hainan University, Haikou, 570228, China

ARTICLE INFO

Keywords:

Cannabidiol
Inulin
Nanoparticles
Multi-targeting
Ulcerative colitis

ABSTRACT

The pathogenesis of ulcerative colitis (UC) is closely related to severe inflammation, damaged colonic mucosal barrier, increased oxidative stress and intestinal ecological imbalance. However, due to the nonspecific distribution and poor bioavailability of drugs, UC treatment is still a serious challenge. Here, a mitochondria/colon dual targeted nanoparticles based on redox response was developed to effectively alleviate UC. Cannabidiol nanoparticles (CBD NPs) with a particle size of 143.2 ± 3.11 nm were prepared by self-assembly using polymers (TPP-IN-LA) obtained by modifying inulin with (5-carboxypentyl) triphenyl phosphonium bromide (TPP) and α -lipoic acid (α -LA). Excitingly, the constructed CBD NPs showed excellent mitochondrial targeting, with a Pearson correlation coefficient of 0.76 at 12 h. The results of animal imaging *in vivo* showed that CBD NPs could be effectively accumulated in colon tissue. Not only that, CBD showed significant glutathione stimulated release in the presence of 10 mM glutathione at pH 7.4. The results of *in vivo* animal experiments showed that CBD NPs significantly ameliorated DSS-induced colonic inflammation by modulating the TLR4-NF- κ B signaling pathway. Moreover, CBD NPs significantly improved the histological damage of colon in UC mice, increased the expression level of tight junction protein ZO-1, and effectively restored the intestinal mucosal barrier function and intestinal mucosal permeability. More importantly, CBD NPs significantly improved the species composition, abundance and amount of short chain fatty acids of intestinal flora in UC mice, thus effectively maintaining the balance of intestinal flora. The dual-targeted and glutathione-responsive nanoparticles prepared in this study provide a promising idea for achieving targeted delivery of CBD for effective treatment of UC.

1. Introduction

Ulcerative colitis (UC) is an incurable inflammatory bowel disease (IBD) characterized by chronic intestinal inflammation, and its symptoms mainly include abdominal pain, diarrhea, weight loss and bloody stool [1]. It has been proved that the pathogenic factors of UC are mainly related to the destruction of intestinal mucosal barrier, the infiltration of inflammatory cells, the increase of oxidative stress level and the imbalance of intestinal microorganisms [2]. In recent years, the incidence rate of UC is increasing rapidly worldwide [3]. Currently, 5-aminosalicylic acid, a first-line therapeutic drug, is used to alleviate the mild symptoms of UC patients [4]. Corticosteroids can be further used to alleviate the moderate symptoms of UC patients who have not been

relieved after 5-ASA treatment [5]. For patients with severe UC, immunosuppressants or biological agents are more effective treatments [6]. However, all of these first-line drugs not only do not completely cure UC but also pose health risks to humans, such as dose-dependent toxicity, complications such as hypertension and gastric ulcers, nephrotoxicity, and an increased risk of malignancy [7]. Therefore, it is urgent to find an effective strategy to deal with the huge challenges of UC treatment.

As one of the oldest plants cultivated by human beings, *Cannabis sativa* L. subsp. *sativa* (cannabis) has been used as a source of fiber, oil and food for thousands of years [8]. Among them, Δ 9-tetrahydrocannabinol (THC) and cannabidiol (CBD) are the most abundant plant cannabinoids in cannabis [9]. Different from THC, as a non euphoric

* Corresponding author. College of Food Science and Engineering, Hainan University, No. 58, Renmin Avenue, Meilan District, Haikou, 570228, China.

E-mail address: shenxuanri2009@163.com (X. Shen).

<https://doi.org/10.1016/j.mtbio.2024.100965>

Received 1 November 2023; Received in revised form 11 January 2024; Accepted 18 January 2024

Available online 19 January 2024

2590-0064/© 2024 The Authors. Published by Elsevier Ltd. This is an open access article under the CC BY-NC-ND license (<http://creativecommons.org/licenses/by-nc-nd/4.0/>).

component of cannabinoid, CBD does not cause any mental effects. More importantly, it has been proved that CBD has significant anti-inflammation, anti-virus, anti-cancer, immune regulation and other effects [10–13], which has been confirmed in pain, inflammation, cardiovascular disease, metabolic disorders, neurodegenerative diseases, cancer and other diseases. In particular, it is worth noting that it has been reported that CBD has shown great potential in effectively alleviating UC [14], manifested by significantly inhibiting the levels of inflammatory factors in colitis tissue and improving colonic mucosal damage. However, due to the poor solubility and its easy decomposition under light, the bioavailability of CBD is low, which severely limits the clinical application of CBD [15]. In order to overcome the above shortcomings, in recent years, strategies based on nanoparticle delivery system have been actively developed to improve the bioavailability of natural active compounds. Nanoparticle delivery systems can be passively targeted to colitis tissues through enhanced epithelial permeability and retention (eEPR) effects [16]. Although the eEPR effect can promote the accumulation of nanoparticles delivery system in colitis tissue, the therapeutic effect of these drugs is still limited by the shortcomings of poor targeting ability and non-specific drug release [17]. Therefore, more effective strategies are needed to achieve targeted drug delivery at the colitis site.

Mitochondria, traditionally recognized as playing an important role in adenosine triphosphate (ATP) production, energy conversion, and maintenance of cellular function and homeostasis, have been shown to be involved in the regulation of inflammatory processes [18]. Studies have shown that the development of UC is closely related to mitochondrial dysfunction [19]. UC patients showed mitochondrial dysfunction, including impaired oxidative phosphorylation, limited ATP generation, and excessive production of reactive oxygen species (ROS) in colonic epithelial cells [20]. The overproduction of ROS leads to lipid, protein and DNA damage within colonic cells and compromises the integrity of the colonic epithelium, further exacerbating the inflammatory process. Therefore, restoration of mitochondrial function is essential not only for energetic homeostasis but also for effective prevention of UC. This also suggests that mitochondria may be a new target organelle for effective treatment of UC. As a lipophilic cation, (5-carboxypentyl) triphenyl phosphonium bromide (TPP) targets mitochondria through electrostatic interaction with negative charges on the cell membrane surface [21]. Based on this principle, TPP is often used as the wall material of mitochondrial targeting for delivering bioactive substances. It can be used as a targeted modified ligand for the effective internalization of nanoparticles to improve intracellular oxidative stress levels and maintain mitochondrial function, thereby enhancing the therapeutic effect of UC. In addition, factors such as pH, redox and enzymes in the inflammatory environment can be used as endogenous stimuli to promote the nanoparticles delivery system to respond to the environment, thus specifically releasing drugs [22]. Among them, in these stimulus responsive nanoparticle delivery systems, redox sensitive nanoparticles containing disulfide bonds have aroused great interest. This is because the high concentration of GSH in inflammatory cells can lead to the breaking of disulfide bond, thus realizing the degradation of nanoparticles and the specific release of drugs [23]. α -lipoic acid (α -LA), as a natural antioxidant, exists widely in plants, animals and human beings [24]. It not only plays an important role in improving glucose metabolism and reducing oxidative stress [25], but also contains disulfide bonds, which can be used as a cross-linking agent to design redox sensitive nanoparticles delivery system [26]. Therefore, based on the above principles, the design of mitochondrial targeted nanoparticle delivery system based on redox response is a more promising method to achieve targeted drug delivery and specific release so as to improve the therapeutic effect of UC.

Compared with other treatments, oral administration has the advantages of good safety, high patient compliance, and direct delivery of drugs to the colon, which is generally considered to be the preferred method for UC treatment [26,27]. However, due to the biochemical and

physiological barriers in the complex environment of gastrointestinal tract (GIT), it may lead to the absorption, degradation and non-specific distribution of drugs in the upper part of GIT before reaching the colitis tissue, thus reducing the therapeutic effect of UC [28]. Therefore, in order to overcome the above challenges, it is essential to find a nano carrier with excellent gastrointestinal stability. Inulin (IN), as a fructose oligosaccharide, is distributed in a variety of vegetables and herbs, which is composed of D-fructose units [29]. Because of its good biocompatibility, excellent safety and biodegradability, IN has been approved for clinical application by the US Food and Drug Administration [30]. It is worth noting that IN will not be digested in the stomach and small intestine so that it can reach the colon smoothly, and then be degraded by the microbiota in the colon [31]. This unique property makes IN a more attractive colon targeting carrier for oral administration. Moreover, IN also plays a probiotic role in colon anaerobic fermentation, promoting the growth of beneficial bacteria and producing short-chain fatty acids (SCFAs), which has a very prominent advantage for the effective treatment of UC [32].

In this study, an oral drug delivery system with multiple-targeting of mitochondria and colon based on redox response was designed to effectively alleviate UC. Here, IN was used as raw material to graft TPP and α -LA respectively to obtain polymer TPP-IN-LA. Polymer TPP-IN-LA can self-assemble in water and successfully encapsulate CBD to obtain CBD NPs. After oral administration, due to its redox response, mitochondrial and colon targeting, CBD NPs can effectively accumulate in colitis tissue, inhibit the production of inflammatory factors, improve the level of oxidative stress, reduce colon tissue injury, restore mucosal barrier, and effectively maintain the homeostasis of intestinal flora and their short-chain fatty acids (SCFAs), thus effectively preventing UC. This multiple targeting strategy can achieve targeted delivery and specific release of drugs in the colon, providing potential candidate drugs for effective treatment of UC.

2. Materials and methods

2.1. Materials

Inulin (IN) was obtained from Shanghai Macklin Biochemical Technology Co., Ltd. (Shanghai, China). The molecular weight (Mw) of IN was measured by high performance gel permeation chromatography (HPGPC) using Waters Alliance 2695 HPLC (Milford, MA, USA) system equipped with Waters Alliance 2414 refractive index detector and TSK-gel G4000 chromatographic column (7.8 mm \times 300 mm). The results showed that the molecular weight of IN was 3265 Da. α -lipoic acid was purchased from Bioengineering (Shanghai) Co., Ltd. (Shanghai, China). (5-carboxypentyl) triphenyl phosphonium bromide (TPP), dicyclohexylcarbodiimide (DCC) and 5-aminosalicylic acid (5-ASA) were purchased from Macklin Biochemical Co., Ltd. (Shanghai, China). Cannabidiol was acquired by Shanghai Aladdin Biochemical Technology Co., Ltd. (Shanghai, China). CB1 receptor inhibitor (R824606) and CB2 receptor inhibitor (SR144528) were purchased from Shanghai Macklin Biochemical Technology Co., Ltd. (Shanghai, China) and Shanghai Jizhi Biochemical Technology Co., Ltd. (Shanghai, China), respectively. Dulbecco's modified eagle medium was provided by Gibco (Life Technologies Corporation, USA). Lipopolysaccharide (LPS) was obtained from Beijing Solarbio Science & Technology Co., Ltd. (Beijing, China). Nitric oxide (NO), nitric oxide synthase (iNOS), reactive oxygen species (ROS), Myeloperoxidase (MPO), catalase (CAT), superoxide dismutase (SOD), malondialdehyde (MDA), adenosine triphosphate (ATP) content, alanine aminotransferase (ALT), aspartate aminotransferase (AST), lactate dehydrogenase (LDH), total bilirubin (T-BIL), uric acid (UA), blood urea nitrogen (BUN), creatinine (CRE) and albumin (ALB) kits were provided by Nanjing Jiancheng Bioengineering Institute (Nanjing, China). Mitochondrial membrane potential (MMP) kit was supplied from Beyotime Institute of Biotechnology (Shanghai, China). Enzyme-linked immunosorbent assay kits, including tumor necrosis factor- α

(TNF- α), interleukin-1 β (IL-1 β), interleukin-4 (IL-4), interleukin-10 (IL-10), platelet activating factor (PAF) and D-lactic acid (D-La) were purchased from Shanghai Xinyu Biotechnology Co., Ltd. (Shanghai, China). Dextran sulfate sodium salt (DSS, molecular weight 36000–50000 Da) was purchased from Yisheng Biotechnology (Shanghai) Co., Ltd. (Shanghai, China).

2.2. Synthesis of polymers

α -Lipoic acid (α -LA) was dissolved in ultra-dry DMSO, then dicyclohexylcarbodiimide (DCC) and 4-dimethylaminopyridine (DMAP) were added and activated at room temperature for 2 h. Then, the DMSO solution of IN was added to the above solution and stirred at room temperature for 72 h. Next, the polymer solution was transferred into a dialysis bag (MWCO 3500 Da) and dialyzed for 24 h. After complete dialysis, the polymer solution was concentrated and lyophilized to obtain the polymer (IN-LA). Then the polymer (TPP-IN-LA) formed by TPP grafted polymer IN-LA was synthesized by the method similar to the above.

2.3. Molecular dynamics simulation

The self-assembly mechanism of the polymers was carried out through molecular dynamics simulations (MD). All simulations and analyses were performed by GROMACS-2022 in the Amber14sb_parmbsc1 all-atom force field. The initial conditions for self-assembly were 20 TPP-IN-LA polymer molecules randomly placed in a $10 \times 10 \times 10 \text{ nm}^3$ box with 30211 water molecules in the system. The temperature during the simulation was coupled to 363 K using the V-rescale method to bring the system to equilibrium quickly. The compressibility was coupled to $4.5 \text{ e-}5$ using the Parrinello-Rahman method, and the covalent bonds were bound by hydrogen atoms. The system was simulated at 20000 ps in the final generated phase to achieve convergence. VMD 1.9.3 was used for image rendering.

2.4. Preparation of nanoparticles

The polymer TPP-IN-LA and cannabidiol (CBD) were dissolved in ultra-dry DMSO together. Then, distilled water was added dropwise to the above mixed solution under uniform stirring. After stirring for 2 h, the nanoparticle suspension was sonicated in an ice bath to disperse uniformly. Next, the homogeneous nanoparticle suspension was transferred into a dialysis bag (12–14 kDa) and dialyzed with excess distilled water for 24 h to remove DMSO. Finally, the obtained solution was centrifuged (4000 rpm, 10 min), filtered with a $0.45 \mu\text{m}$ microporous membrane, and freeze-dried to obtain CBD-loaded nanoparticles (CBD NPs). TPP-IN-LA nanoparticles (Blank NPs) were obtained in a similar method as described above.

2.5. Determination of lysosomal escape behavior

To simulate the lysosomal escape behavior of nanoparticles, FITC-loaded nanoparticles (FITC NPs) were prepared according to the above-mentioned preparation method of CBD NPs. RAW264.7 cells were seeded in laser confocal dishes and adhered for 24 h. Then, cells were co-cultured with FITC, FITC NPs and FITC NPs + GSH for 2 h, 6 h, 12 h. Cells were washed 2–3 times with PBS. Next, cells were stained with the lysosome probe Lyso Tracker Red for 30 min and washed 3 times with PBS. Then, cells were then fixed with 4 % paraformaldehyde for 15 min and washed twice with PBS. Next, the nuclei were stained with DAPI and washed twice with PBS again. Finally, cells were covered with a mixture of PBS and glycerol (1: 9) and observed with a laser scanning confocal microscope (Leica, Wetzlar, Germany).

2.6. Analysis of mitochondrial co-localization

The distribution of FITC NPs in mitochondria was detected using mitochondrial fluorescent probe Mito-Tracker Red (red fluorescence). RAW264.7 cells were inoculated into laser confocal dishes and cultured for 24 h. Then the cells were incubated with FITC NPs for 6 h and 12 h. Then the nucleus and mitochondria were stained with DAPI and Mito-tracker fluorescent probes respectively and washed with PBS 2–3 times. Finally, the images were recorded by laser confocal microscope. The co localization of FITC NPs and mitochondria was evaluated using Pearson correlation coefficient (R). The values of R at 0 and 1 correspond to uncorrelated and fully linear correlation, respectively.

2.7. Determination of anti-inflammatory activity in vitro

Studies have shown that activated neutrophils secrete a large number of inflammatory cytokines, thereby exacerbating the inflammatory state [33]. Based on this, the *in vitro* anti-inflammatory activity of nanoparticles was assessed by measuring the levels of inflammatory factors in cells. RAW264.7 cells were cultured in 12-well plates for 24 h. Then, cells were treated with CBD, CBD NPs and CBD NPs + GSH for 24 h. Next, cells were exposed to LPS ($1 \mu\text{g/mL}$) for 24 h. Inflammatory factor levels (NO, iNOS, TNF- α , IL-1 β , IL-4, and IL-10) in cells were determined using Elisa kits.

2.8. Biodistribution in vivo

To track the *in vivo* biodistribution of nanoparticles, Cy7-loaded nanoparticles (Cy7 NPs) were prepared according to the above-mentioned preparation method of CBD NPs. Balb/c female mice were randomly divided into two groups ($n = 10$), namely, Cy7 and Cy7 NPs. Two groups of mice were orally administered $200 \mu\text{L}$ Cy7 and Cy7 NPs, respectively. Then, the mice were sacrificed by ocular bleeding at different time points (2, 4, 8 and 12 h). Mice were dissected to collect their gastrointestinal tract as well as major organs (heart, liver, spleen, lung and kidney). Photographs were taken using an *in vivo* imaging system to examine the retention and distribution of fluorescence *in vivo*.

2.9. Evaluation of therapeutic effect of nanoparticles on UC in vivo

2.9.1. Experimental design

Ulcerative colitis (UC) was induced by adding dextran sulfate sodium salt (DSS, 3.5 %) to drinking water. All mice were randomly divided into the following groups: (1) Control, (2) DSS group (3.5 % DSS), (3) 5-aminosalicylate (5-ASA, 10 mg/kg) + 3.5 % DSS, (4) free CBD (dosage 10 mg/kg) + 3.5 % DSS, (5) CBD NPs (containing 10 mg/kg of CBD) + 3.5 % DSS. First, all mice were orally administered $200 \mu\text{L}$ of the above sample for 21 days of treatment. From the 15th day, except for the control group, the other groups were treated with DSS in drinking water for 7 days. Body weights of UC mice were recorded every 2 days.

2.9.2. Determination of related indicators in UC mice

On the 22nd day, all mice were sacrificed by ocular bleeding, and blood was collected for analysis of serum oxidative stress levels (PAF, D-La, LDH, CAT, SOD and MDA). The main organs of the mice (heart, liver, spleen, lung and kidney) were collected and weighed to calculate the organ index. At the same time, colon tissue of UC mice was collected to measure colon length as well as colon weight. Disease activity index (DAI) scores of UC mice were assessed by daily monitoring of UC mice for changes in physical signs, namely body weight (0–3), stool consistency (0–3), and rectal bleeding (0–3) [34]. Furthermore, the activity of myeloperoxidase (MPO) and the levels of inflammatory factors (NO, iNOS, TNF- α , IL-1 β , IL-4 and IL-10) in colon tissue were determined by commercial kits. ATP content in colon tissue was determined using an ATP content assay kit. Colon tissue from the same site of UC mice was obtained for histological observation (hematoxylin and eosin (H & E),

Periodic acid-Schiff (PAS) staining). Histological scoring was performed according to three indicators of inflammation severity, crypt damage, and ulceration [35]. The expression of tight junction protein ZO-1 in colon tissue was determined by immunohistochemistry. The expression of NOS2 (M1 biomarker) and CD206 (M2 biomarker) in colon tissue was evaluated by immunofluorescence staining.

2.9.3. Western blotting

Colon tissues (50 mg) were homogenized with RIPA lysate (500 μ L) containing protease inhibitors and phosphatase inhibitors to extract proteins, and then protein concentrations were determined using the BCA protein assay kit. Western blotting of TLR4, MyD88, NF- κ B-p65, p-NF- κ B p65, I κ B α , p-I κ B α , and β -actin was performed. Photographs were taken by a Bio-Rad imaging system (Bio-Rad Laboratories Inc., State of California, USA) and quantitatively analyzed using ImageJ software.

2.9.4. Analysis of intestinal flora

The feces of each group mice before sacrifice were collected in sterilized centrifuge tubes and immediately placed at -80 $^{\circ}$ C for 16s rRNA analysis. The V3-V4 region was amplified by PCR using primers 338F (5'-ACTCCTACGGAGGCA GCAG-3') and 806R (5'-GGACTACHVGGGTTTWTCTAAT-3'). DNA extraction, PCR amplification, fluorescence quantification, Miseq library construction and Miseq library construction were all completed in Shanghai Majorbio Bio-pharm Technology Co. Ltd (Shanghai, China). α -Diversity analysis, species composition analysis, sample comparison analysis, and species difference analysis are performed on the company's cloud platform. Finally, the relevant data of intestinal flora were processed and analyzed.

2.10. Determination of short chain fatty acids

The levels of major SCFAs in mouse feces, including acetic acid, propionic acid and butyric acid, were determined by gas chromatography-mass spectrometry (GC-MS) (Agilent 7890B, USA). In short, 100 mg fecal sample was put into a 2 mL Eppendorf tube and mixed with 20 μ L dilute sulfuric acid (50 %, v/v), then 1 mL ether containing 2-ethylbutyric acid was added and fully ground for 5 min. Next, all samples were sonicated for 30 min in an ice water bath. The sample was then allowed to stand for 30 min at -20 $^{\circ}$ C and centrifuged (12000 g, 15 min). 250 mg anhydrous sodium sulfate was added to the supernatant, mixed and centrifuged (12000 g, 15 min, 4 $^{\circ}$ C). Finally, the supernatant was filtered with a 0.22 μ m microporous membrane, and the content of SCFAs in UC mice was determined by GC-MS.

3. Results and discussion

3.1. Synthesis and characterization of polymers

The polymer TPP-IN-LA was synthesized through a two-step esterification strategy. In the first step, in order to synthesize nano-carrier with redox response, hydrophobic α -lipoic acid (α -LA) was conjugated to hydrophilic IN by esterification to form polymer IN-LA (Fig. 1A). In the second step, in order to further obtain the nano-carrier with mitochondrial targeting, the carboxyl group of TPP was activated by DCC/DMAP for 2 h, and then combined with the hydroxyl group of polymer IN-LA to form a stable polymer TPP-IN-LA. In the 1 H NMR of polymer IN-LA, the signals of 4.06 ppm, 4.62 ppm, 4.72 ppm, 5.18 ppm were assigned to the characteristic peaks of IN (1H, C3-H; 2H, C6-OH; 1H, C3-OH and 1H, C4-OH) (Fig. 1B). The signal of 1.02–1.68 ppm was attributed to the lipoic ring on lipoic acid, while the chemical shift of 1.85–1.91 ppm and 3.18–3.22 ppm corresponded to the disulfide bond on α -LA, demonstrating the successful conjugation of IN and α -LA. These results were consistent with the results reported in the literature [32]. In the 1 H NMR of TPP-IN-LA, the presence of 7.79 ppm and 7.92 ppm signals proved the existence of TPP (Fig. 1B). As shown in Fig. 1C, in the

infrared spectrum of IN-LA, the characteristic peaks of 2929 cm^{-1} and 647 cm^{-1} corresponded to the stretching vibration of $-\text{CH}_2$ and S-S of α -LA, respectively. As expected, a new characteristic peak appeared at 1708 cm^{-1} , which was attributed to the stretching vibration of ester bond. Similarly, the characteristic peak of ester bond also appeared in the infrared spectrum of TPP-IN-LA. The above results indicated that polymer IN-LA and TPP-IN-LA were successfully synthesized. As shown in Fig. 1D, IN contained C and O two elements, while the appearance of S element in polymer IN-LA was attributed to the introduction of α -LA. Also, four elements, C, O, S and P, were observed in TPP-IN-LA, which indicated the successful synthesis of TPP and polymer IN-LA. And the element contents of C, O, S and P in TPP-IN-LA were 73.34 ± 0.34 %, 10.01 ± 0.83 %, 10.65 ± 0.63 % and 0.40 ± 0.04 % respectively (Fig. S1). In addition, obviously, it could be clearly observed that C, O, S and P were uniformly distributed, indicating that α -LA and TPP were connected to IN instead of mixed together (Fig. 1E). The above results strongly proved that polymers IN-LA and TPP-IN-LA were successfully synthesized.

The possible self-assembly mechanism of polymer TPP-IN-LA was analyzed by molecular dynamics (MD) simulations. Under initial conditions, the polymer TPP-IN-LA is dispersed in the system. After equilibrating by molecular dynamics simulation for 20000 ps, polymer TPP-IN-LA could be observed to aggregate together (Fig. 1F). Moreover, the radius of gyration of polymer TPP-IN-LA decreased from 5.4 nm to 2.4 nm during the self-assembly process (Fig. 1G). The solvent-accessible surface area of the polymer decreased with the simulation time (Fig. 1H). And the van der Waals interaction energy and electrostatic interaction energy between TPP-IN-LA gradually decreased throughout the self-assembly process, indicating that the system was gradually stabilized under these two effects (Fig. 1I). The self-assembler also maintains the stability of the system through the hydrogen bonding between TPP-IN-LA (Fig. 1J). All the above indicators show that the amphiphilic polymer TPP-IN-LA can successfully self-assemble in water.

3.2. Preparation and characterization of nanoparticles

Next, using polymer TPP-IN-LA as raw material, blank nanoparticles (Blank NPs) and nanoparticles loaded with CBD (CBD NPs) were prepared (Fig. 2A). The results of TEM and AFM showed that Blank NPs and CBD NPs were uniformly spherical (Fig. 2B and C), and their particle sizes were 127.4 ± 3.23 nm and 143.2 ± 3.11 nm, respectively (Fig. 2D). And their zeta potentials were -8.01 ± 0.36 and -17.57 ± 0.93 mV, respectively (Fig. 2E). To further verify that CBD was successfully encapsulated into nanoparticles, the chemical structures of CBD, Blank NPs, CBD + Blank NPs and CBD NPs were determined by infrared spectrum (Fig. 2F). The results showed that the characteristic peaks of CBD were observed at 3522 cm^{-1} , 3074 cm^{-1} , 2965 cm^{-1} , 2856 cm^{-1} , 1583 cm^{-1} , 1515 cm^{-1} and 1215 cm^{-1} . These characteristic peaks still existed in the infrared spectrum of CBD and CBD + Blank NPs. As expected, the infrared spectrum of CBD NPs was similar to that of Blank NPs, and did not contain the characteristic peaks of CBD, indicating that CBD was successfully encapsulated into nanoparticles. Also, the crystal structures of CBD, Blank NPs, CBD + Blank NP and CBD NPs were characterized by X-ray diffraction (Fig. 2G). Obviously, the characteristic peaks of CBD were found at 10.26 $^{\circ}$, 11.72 $^{\circ}$, 12.40 $^{\circ}$, 13.16 $^{\circ}$, 13.76 $^{\circ}$, 15.00 $^{\circ}$, 17.30 $^{\circ}$, 18.62 $^{\circ}$, 20.58 $^{\circ}$, 22.04 $^{\circ}$, 23.74 $^{\circ}$ and 29.06 $^{\circ}$. These characteristic peaks could still be observed in the mixture of CBD and Blank NPs. Interestingly, these peaks disappear in CBD NPs, indicating that CBD was encapsulated inside the nanoparticles rather than on the surface. The above results indicated that CBD was successfully encapsulated. The encapsulation efficiency and drug loading of CBD NPs measured by HPLC were 59.71 ± 0.71 % and 5.43 ± 0.06 %, respectively.

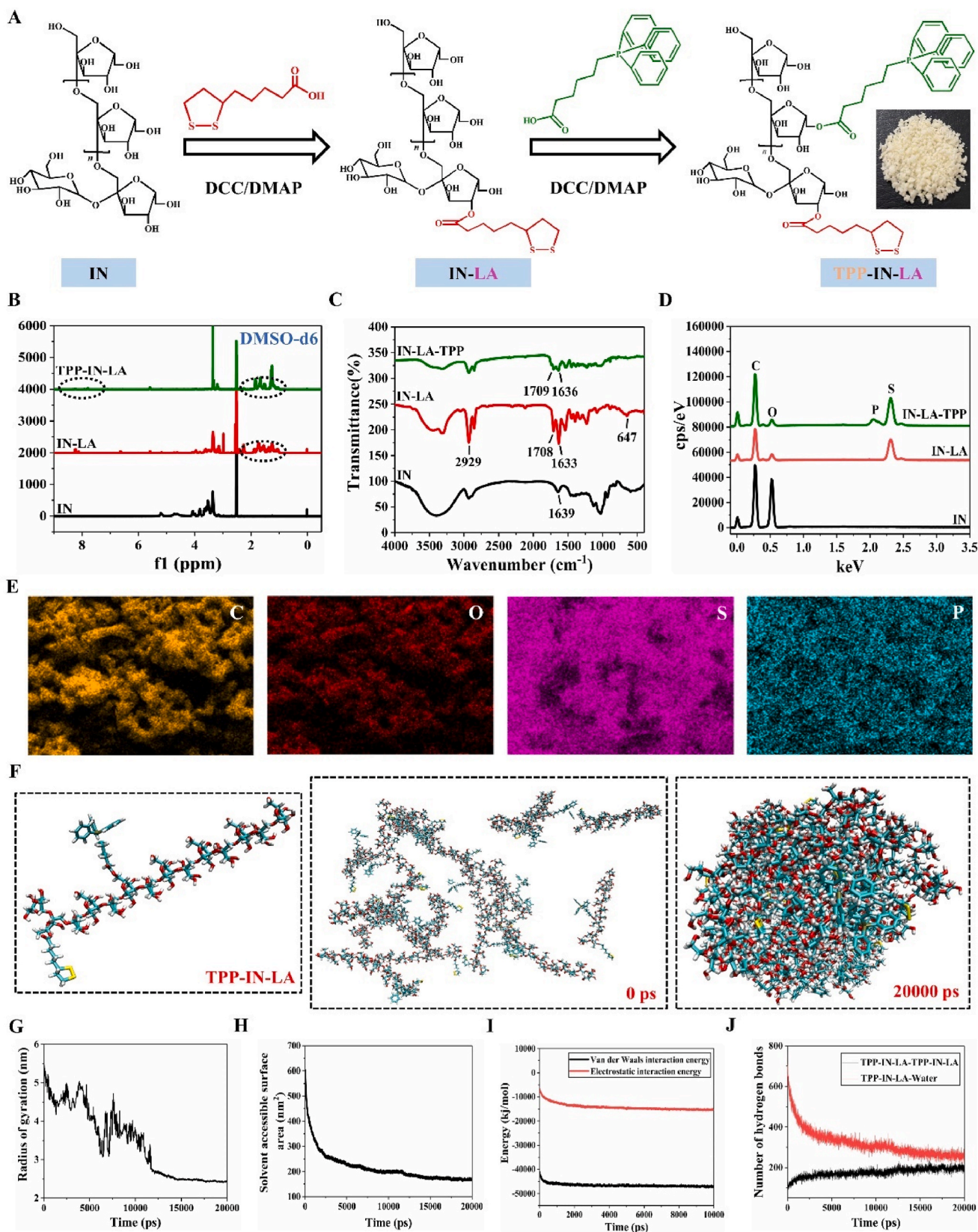


Fig. 1. Preparation and characterization of polymers. (A) Synthesis process of polymer IN-LA and TPP-IN-LA. (B) ^1H NMR spectrum of IN, polymer IN-LA and TPP-IN-LA. (C) Infrared spectrum of IN, polymer IN-LA and TPP-IN-LA. (D) X-ray energy spectrum of element content of IN, polymer IN-LA and TPP-IN-LA. (E) Element distribution of polymer TPP-IN-LA. (F) Self-assembly process of the polymer TPP-IN-LA. (G) Variation of the radius of gyration. (H) Solvent accessible surface area of polymer TPP-IN-LA. (I) Variation of van der Waals and electrostatic interaction energies. (J) Variation of hydrogen bonding.

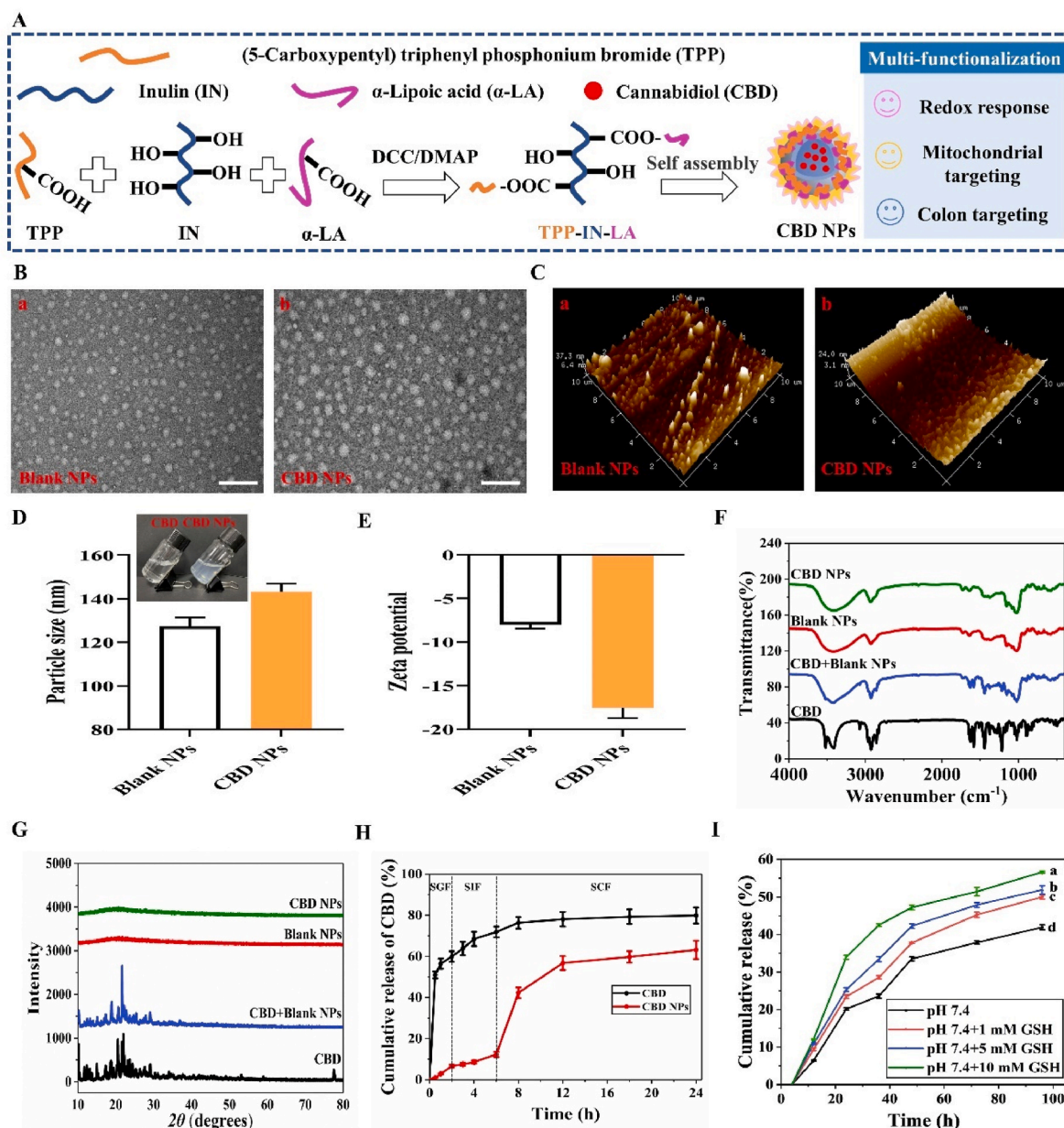


Fig. 2. Preparation and characterization of nanoparticles. (A) Preparation process of CBD NPs. (B) TEM images of Blank NPs (a) and CBD NPs (b). (C) AFM images of Blank NPs (a) and CBD NPs (b). (D) Particle size distribution and (E) zeta potential of Blank NPs and CBD NPs. Illustration: Solubility of CBD and CBD NPs with the same CBD concentration. (F) Infrared spectrum and (G) X-ray diffraction of CBD, Blank NPs, CBD + Blank NPs and CBD NPs. (H) Gastrointestinal stability of CBD NPs. (I) *In vitro* drug release behavior of CBD NPs. Data are mean \pm SD ($n = 3$). * $p < 0.05$, ** $p < 0.01$, *** $p < 0.001$ and **** $p < 0.0001$.

3.3. Gastrointestinal stability of CBD NPs

The stabilities of nanoparticles are very important to ensure that nanoparticles are used in subsequent research. To verify the gastrointestinal stability of nanoparticles, the release of CBD and CBD NPs in simulated gastrointestinal fluid was detected. Obviously, the free CBD diffused rapidly in the simulated gastrointestinal juice, and the cumulative release rates of 59.89 \pm 2.57 %, 11.91 \pm 0.93 % and 8.06 \pm 0.52 % in SGF, SIF and SCF were observed (Fig. 2H). In contrast, the release of CBD NPs in SGF and SIF decreased significantly, and the release rate was 6.66 \pm 0.64 % and 5.64 \pm 0.33 %, respectively, indicating that the nano-carriers prepared in this study could effectively protect CBD from release. Interestingly, the release rate of CBD NPs in SCF significantly increased, indicating that CBD NPs can protect the controlled release of CBD in the colon. The above results show that the constructed nano-carriers had promising characteristics in oral delivery of hydrophobic

bioactive substances.

3.4. *In vitro* drug release characteristics of CBD NPs

In order to study the redox response of CBD NPs, the *in vitro* drug release properties of CBD NPs in PBS solutions containing 1 mM, 5 mM and 10 mM GSH were characterized by dialysis method (Fig. 2I). The results showed that 39.16 \pm 0.49 % of CBD was released by CBD NPs after 96 h at pH 7.4. However, the *in vitro* cumulative release of CBD in nanoparticles was significantly accelerated in the presence of GSH. CBD was released 46 \pm 0.30 %, 49.28 \pm 0.39 % and 54.31 \pm 0.25 % in CBD NPs respectively after 96 h in 1 mM, 5 mM and 10 mM GSH. Obviously, with the increase of GSH concentration, the cumulative release of CBD *in vitro* increased, indicating that the release of CBD in CBD NPs was in a GSH concentration dependent manner. The reason for this phenomenon may be that the disulfide bond in the nanoparticles is broken due to the

high concentration of GSH. The above results proved that the CBD NPs prepared in this study had redox-sensitive properties.

3.5. Determination of CBD concentration

The results of MTT showed that the cell viability was about 10 % when the concentration was higher than 1.5625 $\mu\text{g/mL}$. When cells were treated with CBD at a concentration of 1.5625 $\mu\text{g/mL}$, the cell viability was between 80 and 90 % (Fig. 3D). The cell viability of CBD below this concentration was more than 90 %. Therefore, it is necessary to further study the effect of lower CBD concentration on cell viability. Additionally, in order to facilitate the subsequent experiment, the concentration of CBD was adjusted to 3.2, 1.6, 0.8, 0.4, 0.2, 0.1 $\mu\text{g/mL}$, and then the cytotoxicity of CBD was determined again by MTT method. The results showed that cell viability treated with CBD at 3.2 and 1.6 $\mu\text{g/mL}$ was consistent with the results of cell viability at 3.125 and 1.5625 $\mu\text{g/mL}$ described above (Fig. 3E). Interestingly, when the concentration of CBD was ≤ 0.8 $\mu\text{g/mL}$, the cell viability was more than 90 %, indicating that the CBD below this concentration had no cytotoxicity. Next, the CBD anti-inflammatory activity of 0.8 and 0.4 $\mu\text{g/mL}$ was further determined by NO content. The results showed that both concentrations of CBD could significantly inhibit the production of NO in cell supernatant (Fig. 3F). As expected, the NO content of cells treated with 0.8 $\mu\text{g/mL}$ CBD was much lower than that treated with 0.4 $\mu\text{g/mL}$ CBD. Based on the above experiments, the concentration of CBD was determined to be 0.8 $\mu\text{g/mL}$, and the subsequent cell experiments were carried out with CBD NPs with the same concentration of CBD.

3.6. Cellular uptake of nanoparticles

Subsequently, cell uptake behavior was investigated by treating RAW264.7 cells with FITC, FITC NPs, and FITC NPs + GSH (Fig. 3A). The results showed that the cells treated with FITC NPs showed strong green fluorescence, which was much higher than that of free FITC (Fig. 3B). When pretreated with GSH for 2 h, FITC NPs had stronger cell uptake ability, which was attributed to the fact that higher concentration of GSH could lead to the breaking of disulfide bond in nanoparticles, thus leading to the rapid release of drugs. This result was consistent with the research report of Yang et al. [36]. In addition, the fluorescence intensities of free FITC, FITC NPs, and FITC NPs + GSH were 165.50 ± 4.72 , 194.41 ± 5.11 and 222.41 ± 5.49 (Fig. 3G), respectively, which confirmed the above conclusion. The above results indicated that FITC NPs + GSH had stronger cell uptake capacity.

3.7. Lysosomal escape of nanoparticles

In order to verify that nanoparticles can escape from lysosomes after entering cells, the lysosomal escape behavior of FITC NPs was examined by laser confocal microscopy. Yellow fluorescence indicated that nanoparticles were trapped in the lysosome, while green fluorescence signals represent nanoparticles outside the lysosome. After 2 h of treatment, yellow fluorescence signals were observed, indicating that most FITC NPs were trapped in lysosomes at this time (Fig. 3C). With the extension of time, the yellow fluorescence weakened, and the red fluorescence and green fluorescence gradually separated, indicating that more and more FITC NPs were escaping from the lysosome. At this time, Pearson's correlation coefficient decreased from 0.87 to 0.70. After 12 h of treatment, there was strong green fluorescence outside the lysosome, indicating that most FITC NPs had escaped from the lysosome. At the same time, Pearson's correlation coefficient decreased to 0.27, which also proved the above conclusion.

3.8. Mitochondrial targeting ability of nanoparticles

Because mitochondria are the main site of ROS production, nanoparticles targeting mitochondria can effectively reduce ROS levels,

thereby reducing intracellular inflammation and oxidative stress damage. In order to verify whether nanoparticles can target mitochondria after escaping from lysosomes, the mitochondrial co-localization ability of FITC NPs was analyzed. The results showed that the red fluorescence and green fluorescence were separated at 6 h, and the Pearson's correlation coefficient was -0.24 (Fig. 3J). At 12 h, strong yellow fluorescence was observed, and Pearson's correlation coefficient (0.76) also increased significantly, indicating that nanoparticles grafted with TPP had excellent mitochondrial targeting and accumulation capacity.

3.9. Anti-inflammatory activity of nanoparticles in vitro

As expected, CBD and CBD NPs could significantly inhibit the levels of inflammatory factors NO, iNOS, TNF- α and IL-1 β in cells, and effectively promote the production of anti-inflammatory factors IL-4 and IL-10, indicating that CBD and CBD NPs had significant anti-inflammatory activity (Fig. 3H and I and Fig. 3K-N). It could be observed that the anti-inflammatory effect of CBD NPs was much better than that of CBD, which may be due to the enhanced uptake of CBD NPs in cells. In addition, the anti-inflammatory activity of CBD NPs + GSH was further increased, which may be due to the fact that after pretreatment with GSH for 2 h, higher concentrations of GSH in cells induced the disulfide bond breaking in CBD NPs, thus accelerating the degradation of nanoparticles and drug release.

3.10. Ability of nanoparticles to regulate oxidative stress

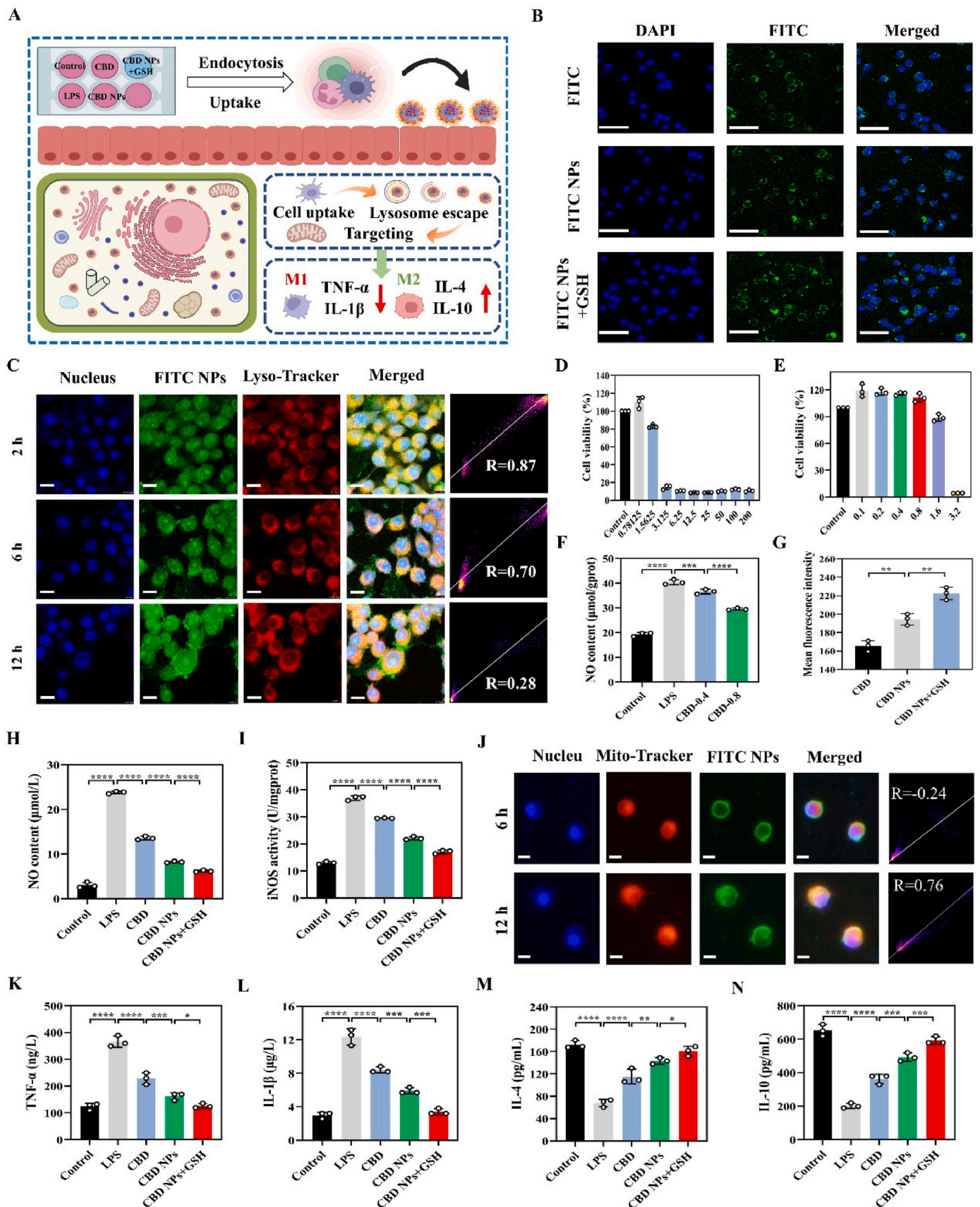
Studies have shown that inflammation not only generates excessive ROS and MPO, leading to severe oxidative stress, but also releases excessive LDH [37]. The imbalance of oxidative stress level will further lead to the reduction of SOD level. Therefore, in this study, the level of oxidative stress in RAW264.7 cells was measured. LPS group showed strong green fluorescence, indicating that cells without any sample treatment had obvious inflammatory damage (Fig. 4A). Interestingly, after the treatment of CBD and CBD NPs, ROS in cells could be effectively removed. After pretreatment with GSH for 2 h, the fluorescence signal of ROS in cells could hardly be detected, which was similar to the control group. This result was verified by the quantitative determination of ROS fluorescence intensity and the ROS level in cells treated with different samples (Fig. S2 and Fig. 3B). Moreover, after treatment with CBD, CBD NPs and CBD NPs + GSH, the levels of MPO and LDH decreased significantly, while the level of SOD increased significantly, suggesting that they could effectively regulate the oxidative stress response in cells (Fig. 4C-E). Notably, it was found that Blank NPs had no significant anti-oxidative stress effect ($p > 0.05$).

3.11. Determination of MMP levels

The level of MMP in cells can reflect the serious damage in cells to a certain extent. Therefore, next, the changes of MMP in RAW264.7 cells were observed and recorded by fluorescence inverted microscope. The results showed that the LPS group had weak red fluorescence and strong green fluorescence, indicating that the cells had inflammatory damage and early apoptosis (Fig. 4F). Not surprisingly, after treatment with CBD and CBD NPs, the red fluorescence in cells increases and the green fluorescence decreases, indicating that they could effectively improve the level of MMP. In particular, the fluorescence signal of CBD NPs + GSH group was almost close to the normal level, indicating that it had a better ability to effectively maintain the balance of MMP. Furthermore, the red/green fluorescence intensity ratio was quantified and similar results were obtained (Fig. S3).

3.12. Changes in ATP content in cells

The above results demonstrated that the prepared nanocarrier targeted mitochondria and significantly maintained the balance of MMP. In



(caption on next page)

Fig. 3. Determination of mitochondrial targeting ability and anti-inflammatory activity of nanoparticles. (A) Flow chart of transport and absorption of CBD NPs in cells. (B) Cell uptake images of RAW264.7 cells processed by FITC, FITC NPs and FITC NPs + GSH. Magnification: 20 times. Scale bar: 60 μm . (C) The fluorescence images of lysosomal escape of FITC NPs at different time points. Scale bar: 20 μm . (D) The cytotoxicity of RAW264.7 cells treated with CBD of 200, 100, 50, 25, 12.5, 6.25, 3.125, 1.5625 and 0.78125 $\mu\text{g}/\text{mL}$, respectively. (E) The cytotoxicity of RAW264.7 cells treated with CBD of 3.2, 1.6, 0.8, 0.4, 0.2, 0.1 $\mu\text{g}/\text{mL}$, respectively. (F) The content of NO in the supernatant of RAW264.7 cells treated with CBD of 0.8 and 0.4 $\mu\text{g}/\text{mL}$. (G) Mean fluorescence intensity of uptake of RAW264.7 cells processed by CBD, CBD NPs and CBD NPs + GSH. The contents of (H) NO and (I) iNOS in the supernatant of RAW264.7 cells treated with CBD, CBD NPs and CBD NPs + GSH. (J) Mitochondrial Co localization analysis of FITC NPs. Magnification: 40 times. Scale bar: 20 μm . The contents of (K) TNF- α , (L) IL-1 β , (M) IL-4 and (N) IL-10 in the supernatant of RAW264.7 cells treated with CBD, CBD NPs and CBD NPs + GSH. Data are mean \pm SD (n = 3). * p < 0.05, ** p < 0.01, *** p < 0.001 and **** p < 0.0001.

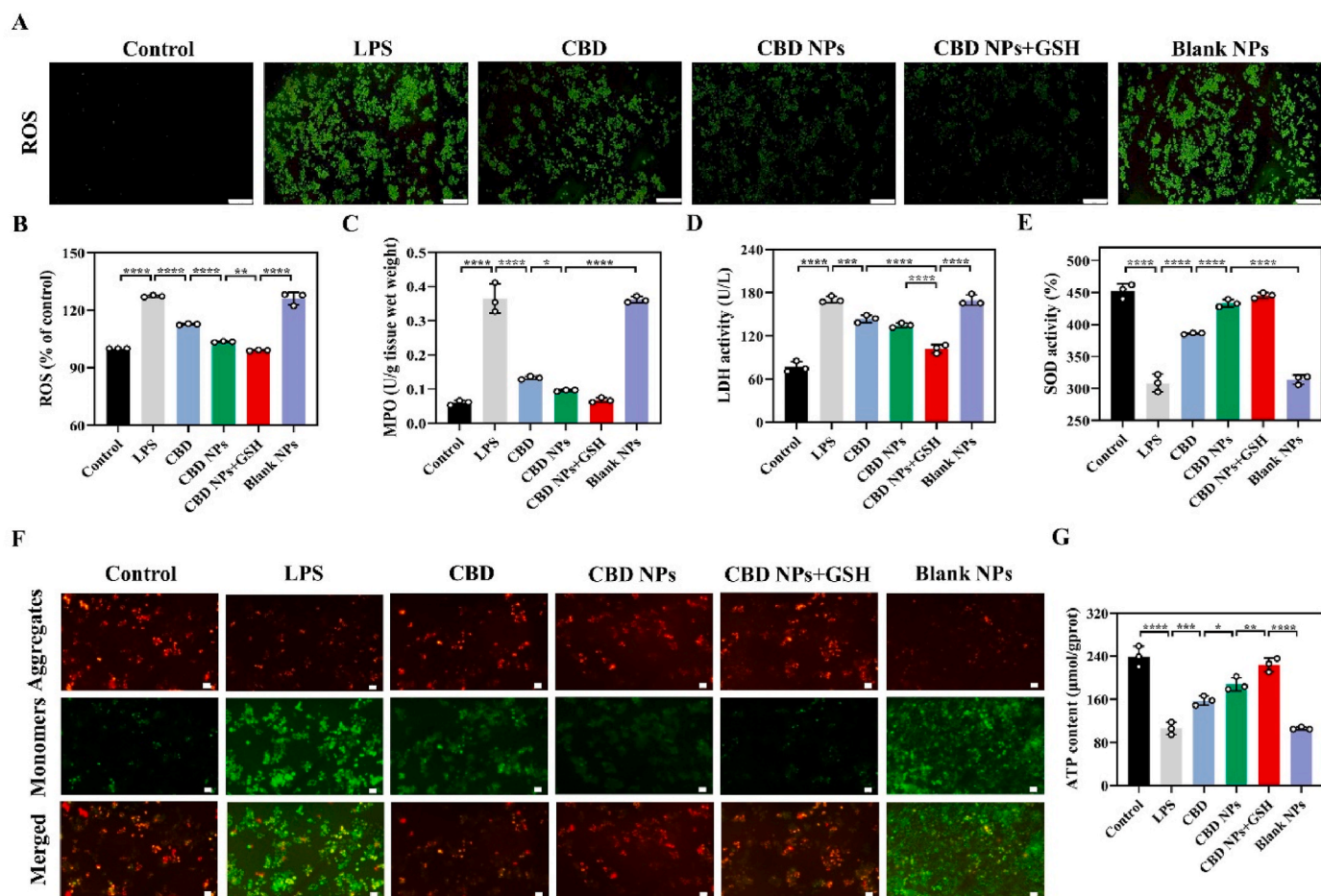


Fig. 4. The ability of nanoparticles to regulate the level of oxidative stress. (A) Fluorescent images representing ROS level in RAW264.7 cells processed by CBD, CBD NPs, CBD NPs + GSH and Blank NPs. Magnification: 10 times. Scale bar: 200 μm . The levels of (B) reactive oxygen species (ROS), (C) myeloperoxidase (MPO), (D) lactate dehydrogenase (LDH) and (E) superoxide dismutase (SOD) in RAW264.7 cells treated with CBD, CBD NPs, CBD NPs + GSH and Blank NPs. (F) Fluorescence intensity images of mitochondrial membrane potential in RAW264.7 cells treated by CBD, CBD NPs, CBD NPs + GSH and Blank NPs. Magnification: 10 times. Scale bar: 20 μm . (G) Changes in ATP content in mitochondria. Data are mean \pm SD (n = 3). * p < 0.05, ** p < 0.01, *** p < 0.001 and **** p < 0.0001.

order to further investigate the effect of nanoparticles on mitochondrial function, the changes of ATP content in RAW264.7 cells treated with CBD, CBD NPs, or CBD NPs + GSH treatment were measured. Obviously, after LPS treatment, RAW264.7 cells showed a significant decrease in ATP content, indicating impaired mitochondrial function. CBD and CBD NPs significantly improved ATP levels in RAW264.7 cells (Fig. 4G). As expected, compared to free CBD, CBD NPs exhibited stronger mitochondrial protective effects, which was due to the fact that CBD NPs could target into mitochondria, thus effectively improving the function of mitochondria. Notably, the pretreatment of GSH further enhanced the protective effect of CBD NPs on mitochondria. The above results indicated that CBD NPs could effectively maintain the balance of MMP, promote the production of ATP molecules in mitochondria, and restore mitochondrial function, thus effectively reducing inflammation.

3.13. Biological distribution of nanoparticles in vivo

The key of UC mice after oral administration is that the drug can accumulate specifically in the inflamed colon tissues. Therefore, in this study, the biodistribution of the drug in UC mice was assessed by removing the gastrointestinal tract as well as major organs at different time points and taking fluorescence images with a living animal imager. Fig. 5A and B showed brightfield images of the gastrointestinal tract as well as major organs. The fluorescence signals of Cy7 and Cy7 NPs increased significantly with the extension of time (Fig. 5C). After 4 h of administration, the fluorescence intensity of Cy7 reached the maximum. While, Cy7 NPs had the strongest fluorescence signal at 8 h, indicating that the nanocarriers prepared in this study could effectively prevent premature degradation of drugs. In addition, Cy7 NPs had stronger colon fluorescence intensity than Cy7, indicating that Cy7 NPs could achieve

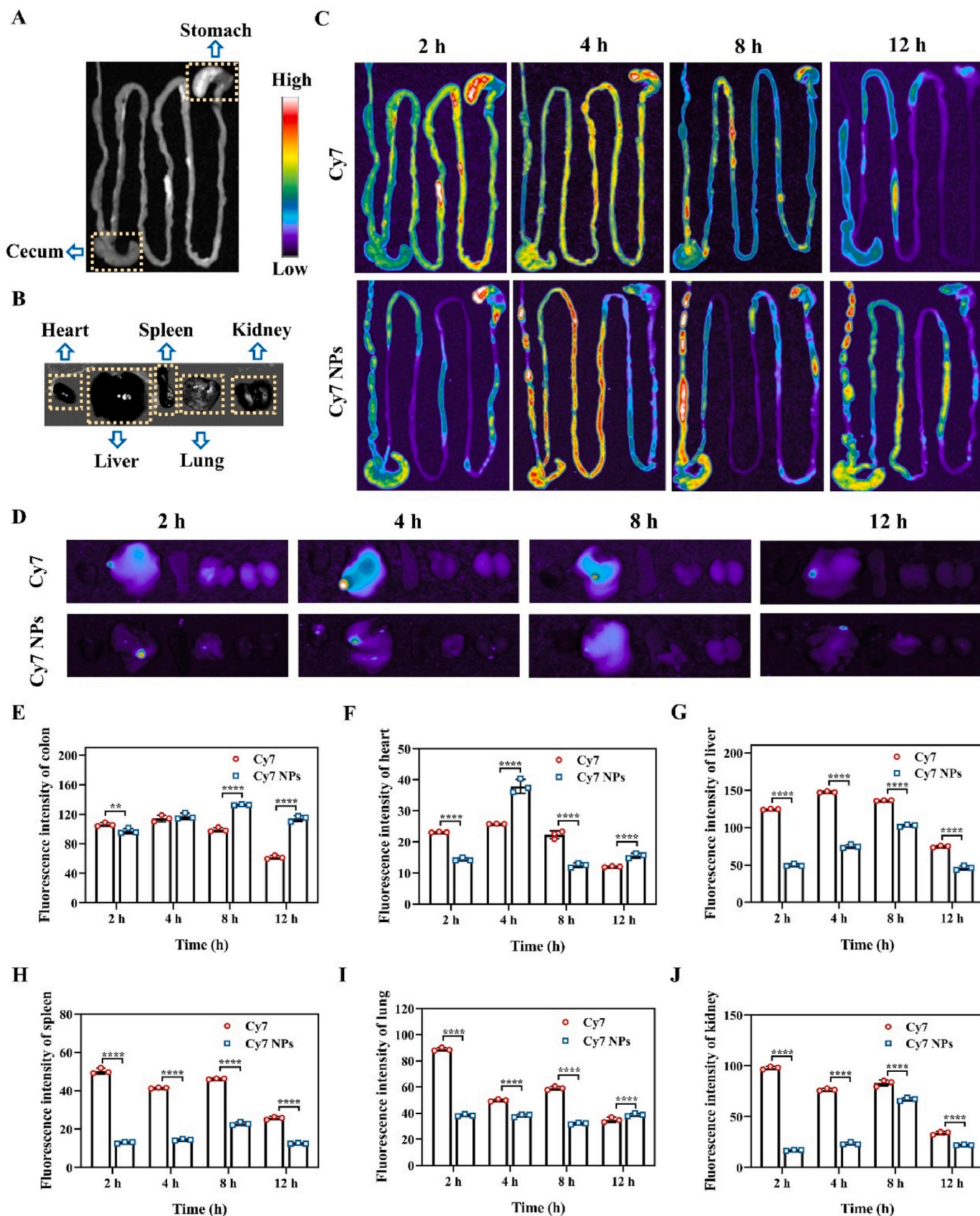


Fig. 5. Biological distribution of nanoparticles *in vivo*. Brightfield images of (A) the gastrointestinal tract and (B) major organs. (C) The fluorescent images of gastrointestinal tract of UC mice processed by Cy7 and Cy7 NPs. (D) The fluorescent images of main organs of UC mice processed by Cy7 and Cy7 NPs. Fluorescence intensity of (E) colon, (F) heart, (G) liver, (H) spleen, (I) lung and (J) kidney processed by Cy7 and Cy7 NPs. Data are mean \pm SD (n = 3). * p < 0.05, ** p < 0.01, *** p < 0.001 and **** p < 0.0001.

specific accumulation of drugs at colonic inflammatory sites. Besides, Cy7 had very weak fluorescence signal at 12 h, while Cy7 NPs still had strong fluorescence intensity at 12 h, indicating that the nanocarrier prepared in this study could effectively increase the drug circulation time in the colon. Furthermore, the fluorescence signals of heart, liver, spleen, lung and kidney of UC mice treated with Cy7 and Cy7 NPs were also observed. The results showed that Cy7 and Cy7 NPs had relatively strong fluorescence intensity of liver and kidney compared with heart, spleen and lung (Fig. 5D). Moreover, Cy7 had stronger liver and kidney fluorescence intensity than Cy7 NPs, indicating that more Cy7 entered the systemic circulation and was metabolized and eliminated by the liver and kidney. In order to further compare the fluorescence intensity, the fluorescence intensity of colon and main organs was quantified, and the results were shown in Fig. 5E–J. The results of fluorescence quantification once again proved the above conclusion.

Furthermore, to demonstrate the colon-targeting ability of Cy7 NPs, we also compared the fluorescence intensities of liver and colon (Figs. S4A–B). The results showed that the fluorescence intensity of free Cy7 in the liver was much higher than that in the colon, indicating that most of the free Cy7 entered the systemic circulation and was metabolized *in vivo*. Surprisingly, regardless of the time point, the fluorescence intensity of Cy7 NPs in the colon was significantly higher than that in the liver, indicating that most Cy7 NPs were effectively targeted to colitis tissue and released the drug without being absorbed into the systemic circulation. The above results strongly demonstrated that the nanocarriers constructed in this study had good colon targeting ability, which was of great significance for the next study on the preventive effect of Cy7 NPs on DSS-induced UC.

3.14. Preventive effect of nanoparticles on UC *in vivo*

Next, in order to verify the therapeutic effect of nanoparticles on UC, mice were given corresponding drugs orally for 21 days, and the experimental process was shown in Fig. 6A. The results showed that the weight of UC mice in the DSS group was significantly reduced (Fig. 6B), and the UC mice in the DSS group had obvious diarrhea and hematochezia, resulting in a higher DAI score (Fig. 6C). It was clear that CBD and CBD NPs not only effectively maintained the weight of UC mice, but also alleviated severe diarrhea and blood in the stool of UC mice. Therefore, the CBD and CBD NPs groups had lower DAI scores. Also, UC mice in the CBD and CBD NPs groups had longer colon length and larger colon index (Fig. 6D–F). In addition, the spleen of UC mice in DSS group showed black swelling (Fig. 6G), resulting in an increase in spleen weight (Fig. 6H). Meanwhile, the liver index and spleen index of DSS group increased (Fig. 6I). The liver index and spleen index in CBD and CBD NPs groups decreased, indicating that they had an effective relieving effect on hepatosplenomegaly.

3.15. Anti-inflammatory activity of nanoparticles *in vivo*

Studies have shown that due to the infiltration of neutrophils in the inflammatory area of the colon, the activity of MPO and the level of proinflammatory cytokines (NO, iNOS, TNF- α and IL-1 β) are increased, which are considered as key indicators related to the degree of inflammation [38,39]. The results showed that the MPO activity and the levels of pro-inflammatory factors (NO, iNOS, TNF- α , IL-1 β) in the DSS group were significantly increased, and the levels of anti-inflammatory factor (IL-4 and IL-10) were significantly decreased (Fig. 7A–G). There was no significant difference between the Blank NPs group and the DSS group, indicating that the Blank NPs had no therapeutic effect on UC. As expected, CBD and CBD NPs significantly decreased the levels of pro-inflammatory factors and increased the levels of anti-inflammatory factors. Among them, the anti-inflammatory activity of CBD NPs was much higher than that of CBD. The reason may be that the solubility of free CBD was poor, the metabolism was fast in the body, and it was quickly cleared by the human body, resulting in poor bioavailability of

free CBD.

3.16. Regulation of nanoparticles on oxidative stress *in vivo*

Studies have shown that in addition to suppressing inflammation that can alleviate UC, antioxidant stress has also been shown to promote the intestinal immune barrier and reduce colitis [40]. Research shows that platelet activating factor (PAF) is a kind of bioactive lipid, which can promote the production of oxygen free radicals. When inflammation occurs in the colon, the level of PAF will increase. Therefore, next, in addition to measuring the content of LDH, CAT, SOD and MDA in serum, we also measured the level of PAF in serum. As shown in Fig. 7H–L, of note, after treatment with CBD and CBD NPs, the concentrations of PAF, LDH and MDA in serum decreased, while the levels of CAT and SOD increased, indicating that CBD and CBD NPs could effectively reduce oxidative stress injury and alleviate the symptoms of UC. Interestingly, CBD NPs showed a more prominent effect in regulating the level of oxidative stress than CBD, which was consistent with the above anti inflammation results *in vivo*. In addition, it could be found that Blank NPs had no significant ameliorating effect on the level of oxidative stress in UC mice.

3.17. Changes in ATP content in colon tissue

Dysregulation of mitochondrial function has been identified in the context of UC, contributing to the perpetuation of inflammation and cellular stress within the colonic tissues. Based on this, the mitochondrial ATP content in colon tissue was measured to evaluate whether CBD NPs can alleviate UC by restoring mitochondrial function. Compared with the control group, a significant decrease in ATP levels was detected in UC mice in the DSS group (Fig. S5), but CBD NPs weakened this ATP decrease, indicating that CBD NPs could effectively promote the production of ATP molecules in mitochondria. The above results demonstrated that CBD NPs could effectively alleviate UC by effectively restoring mitochondrial function and maintaining mitochondrial function and homeostasis.

3.18. Recovery of mucosal barrier function by nanoparticles

Studies have shown that the content of D-La in the peripheral blood is an important indicator to reflect the damage of intestinal mucosal barrier and intestinal mucosal permeability [41]. Therefore, the content of D-La in serum of UC mice was determined to evaluate the recovery ability of nanoparticles on mucosal barrier function of UC mice. The results showed that the content of D-La increased significantly after DSS treatment (Fig. S6). As expected, CBD and CBD NPs significantly reduced the content of D-La in serum, indicating that CBD and CBD NPs can effectively restore the intestinal mucosal barrier function.

3.19. Histological analysis

In order to further evaluate the effect of nanoparticles on the restoration of intestinal mucosal barrier function, H & E staining of colon tissue was performed. It could be clearly observed that CBD and CBD NPs significantly increased the number of goblet cells, reduced the destruction of crypts, and restored the integrity of intestinal mucosa (Fig. 6K). The histological score proved the above conclusion (Fig. 6J). Furthermore, the amount of mucin in colon tissue was detected by PAS staining. As shown in Fig. 6L, compared with the control group, the mucin content of DSS mice was significantly reduced, which was consistent with the result that the goblet cells containing mucus were destroyed observed in H & E staining. The treatment of CBD and CBD NPs was helpful to restore mucin secretion in colon tissue, which was close to that of healthy control. Moreover, tight junctions between cells are very important for maintaining the integrity of the mucosal barrier. Therefore, the expression of tight junction protein ZO-1 in colon tissue

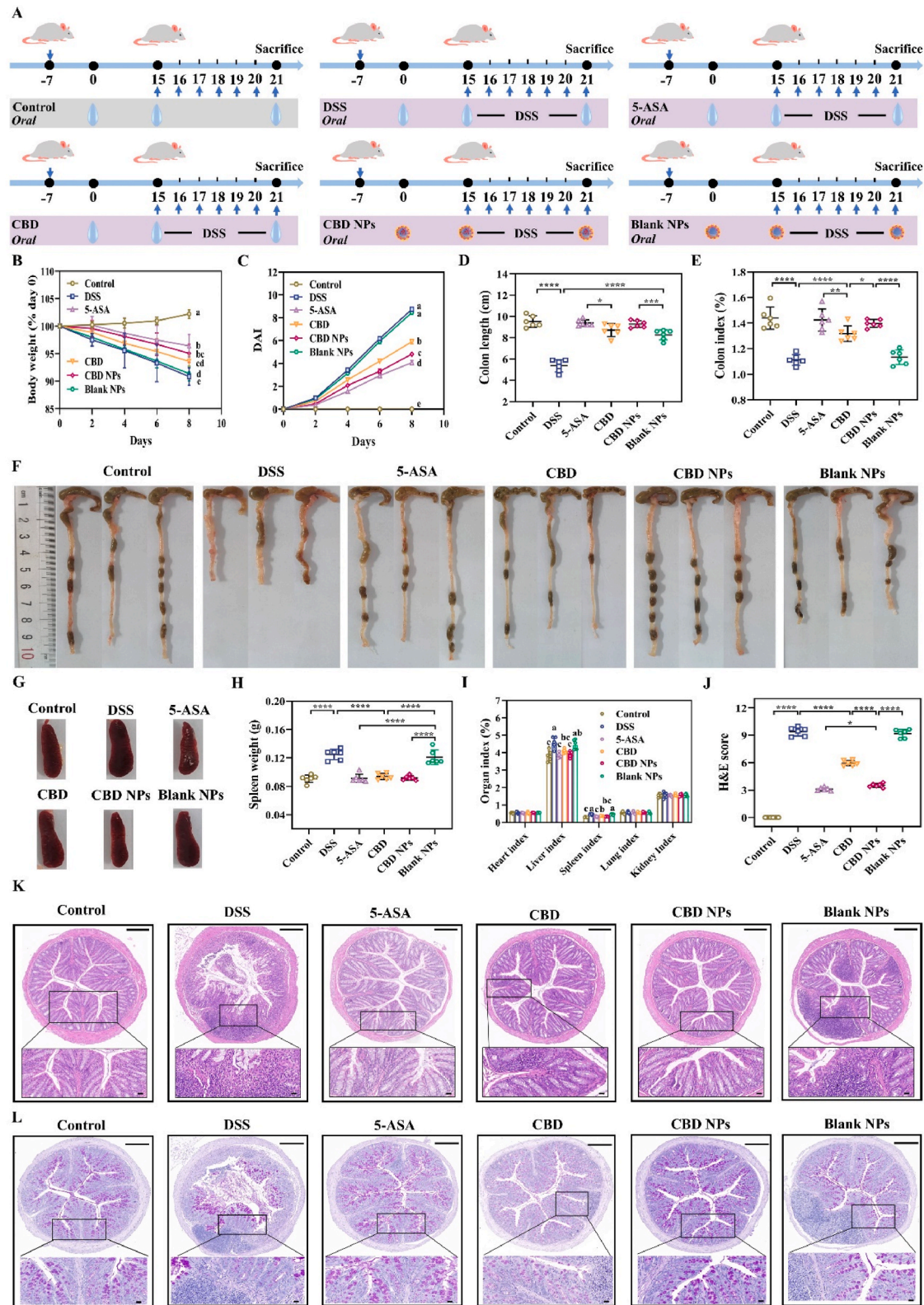


Fig. 6. Preventive effect of nanoparticles on DSS induced UC. (A) Experimental scheme of DSS induced UC. (B) Body weight change, (C) DAI score, (D) colon length, (E) colon index, (F) colon images, (G) spleen images, (H) spleen weight and (I) organ index of UC mice treated with different samples. Different letters in each column represent significant differences between groups ($p < 0.05$). (J) Histological score of colon tissue of UC mice treated with different samples. (K) Hematoxylin and eosin (H & E) images of colon tissue of UC mice treated with different samples. Magnification: 5 and 40 times. Scale bar: 200 μm and 20 μm . (L) Periodic acid-Schiff (PAS) staining images of colon tissue of UC mice treated with different samples. Magnification: 5 and 40 times. Scale bar: 200 μm and 20 μm . Data are mean \pm SD ($n = 6$). * $p < 0.05$, ** $p < 0.01$, *** $p < 0.001$ and **** $p < 0.0001$.

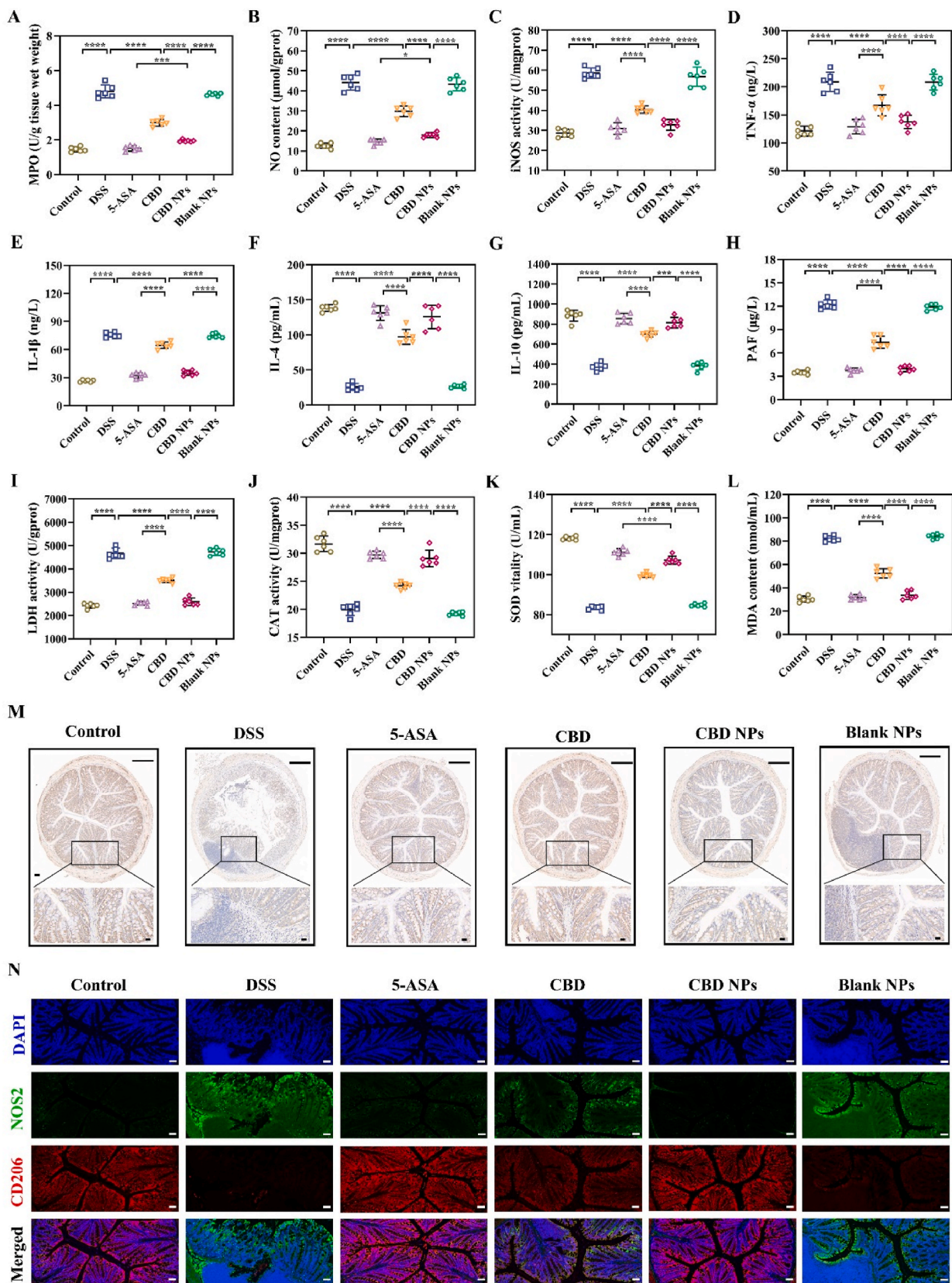


Fig. 7. Anti-inflammatory activity of nanoparticles *in vivo*. The levels of (A) myeloperoxidase (MPO), (B) nitric oxide (NO), (C) nitric oxide synthase (iNOS) and (D) tumor necrosis factor-α (TNF-α), (E) interleukin 1β (IL-1β), (F) interleukin 4 (IL-4), (G) interleukin 10 (IL-10), (H) platelet activating factor (PAF), (I) lactate dehydrogenase (LDH), (J) catalase (CAT), (K) superoxide dismutase (SOD) and (L) malondialdehyde (MDA) in the serum of UC mice treated with different samples. (M) Immunohistochemical analysis of ZO-1 expression in colon tissue of UC mice treated with different samples. Magnification: 5 and 40 times. Scale bar: 200 μm and 20 μm. (N) Immunofluorescence staining image of NOS2 and CD206 expression in colon tissue of UC mice. Magnification: 20 times. Scale bar: 200 μm. Data are mean ± SD (n = 6). **p* < 0.05, ***p* < 0.01, ****p* < 0.001 and *****p* < 0.0001.

was evaluated by immunohistochemistry. The results showed that the expression level of ZO-1 in DSS group was significantly lower than that in control group (Fig. 7M). However, the ZO-1 positive region of UC mice treated with CBD and CBD NPs was significantly larger than that of DSS group, which meant that CBD and CBD NPs reduced the colon mucosal barrier damage of UC mice by increasing the expression of ZO-1. In particular, CBD NPs were more effective than CBD in restoring intestinal mucosal barrier function. Furthermore, in order to evaluate the transformation of M1 to M2 phenotypes *in vivo*, the expression of NOS2 and CD206 in colon tissue was studied by immunofluorescence staining. The results showed that CBD NPs significantly decreased the expression of NOS2 in colon tissues and increased the expression of CD206 (Fig. 7N), indicating that there was an obvious transformation of M1 to M2 phenotype *in vivo*. All the above results proved that CBD NPs effectively alleviated the symptoms of UC, significantly regulated the levels of inflammatory factors and oxidative stress, and effectively restored the barrier function of intestinal mucosa.

3.20. Mechanism of CBD NPs effective in preventing UC

Studies have shown that the mechanism of UC is mainly due to the large amount of LPS in the intestine recognized by Toll-like receptor 4 (TLR4), which activates the downstream inflammatory signaling pathway of NF- κ B by recruiting MyD88 [42]. Under normal conditions, NF- κ B binds to inhibitors of nuclear factor- κ B (I κ B) and exists in an inactive form in the cytoplasm. Upon stimulation, I κ B is phosphorylated and NF- κ B separates from I κ B, leading to its translocation from the cytoplasm to the nucleus and causing inflammatory cytokine secretion (Fig. 8A). As shown in Fig. 8B–F, the protein expression levels of TLR4 and MyD88 as well as phosphorylated NF- κ B and I κ B α were significantly increased in the DSS group, indicating the activation of NF- κ B. CBD NPs significantly down-regulated the expression levels of these proteins, showing a superior effect compared to others. The above results suggested that CBD NPs could exert desirable anti-inflammatory activity by regulating the TLR4-NF- κ B signaling pathway.

3.21. Effect of nanoparticles on intestinal flora of UC mice

More and more evidence has shown that the imbalance of intestinal flora seriously affects the occurrence and progress of UC [43]. Therefore, next, in order to determine the role of CBD NPs in regulating intestinal flora, the changes of intestinal flora in UC mice were analyzed by 16S rRNA sequencing. First of all, the diversity and richness of the community were evaluated by measuring the α diversity (shannon index, simpson index, chao index and ace index) of intestinal flora of UC mice. There was no significant difference in α -diversity between DSS group and Blank NPs group (Fig. 9A–D). However, CBD and CBD NPs had higher shannon index, lower simpson index, higher chao index and ace index than DSS group, indicating that the treatment of CBD and CBD NPs significantly increased the diversity and richness of intestinal microflora in UC mice, resulting in higher α -diversity. The α -diversity of CBD NPs was obviously better than that of CBD.

The results of UpSet venn diagram showed that compared with DSS group, CBD and CBD NPs increased the number of species to 241 and 257, respectively (Fig. 9E). Among them, the number of species of CBD NPs even exceeded that of 5-ASA group (255). Next, the dominant species and their relative abundance in the intestinal flora of UC mice in each group at the genus level were analyzed by the community composition Bar chart and community composition pie chart. The results showed that the control group was mainly composed of *Lactobacillus*, *norank_f_Muribaculaceae*, *Bacteroides*, *Odoribacter*, *Lachnospiraceae* and *Lachnospiraceae_NK4A136_group* (Fig. 9F and Fig. S7). Compared with the control group, the levels of *Lactobacillus* and *norank_f_Muribaculaceae* in DSS group decreased significantly, while the levels of *Bacteroides* and *Desulfovibrio* increased significantly. Previous studies have shown that *Bacteroides* and *Desulfovibrio* are closely related to UC [44]. After CBD and CBD NPs treatment, the levels of *Lactobacillus* and *norank_f_Muribaculaceae* increased significantly, while the levels of *Bacteroides* and *Desulfovibrio* decreased significantly, indicating that CBD and CBD NPs could significantly increase the beneficial flora and inhibit the formation of harmful bacteria. It was worth noting that the beneficial effect of CBD on the regulation of intestinal flora in UC mice was much lower than that of CBD NPs, which was consistent with the results

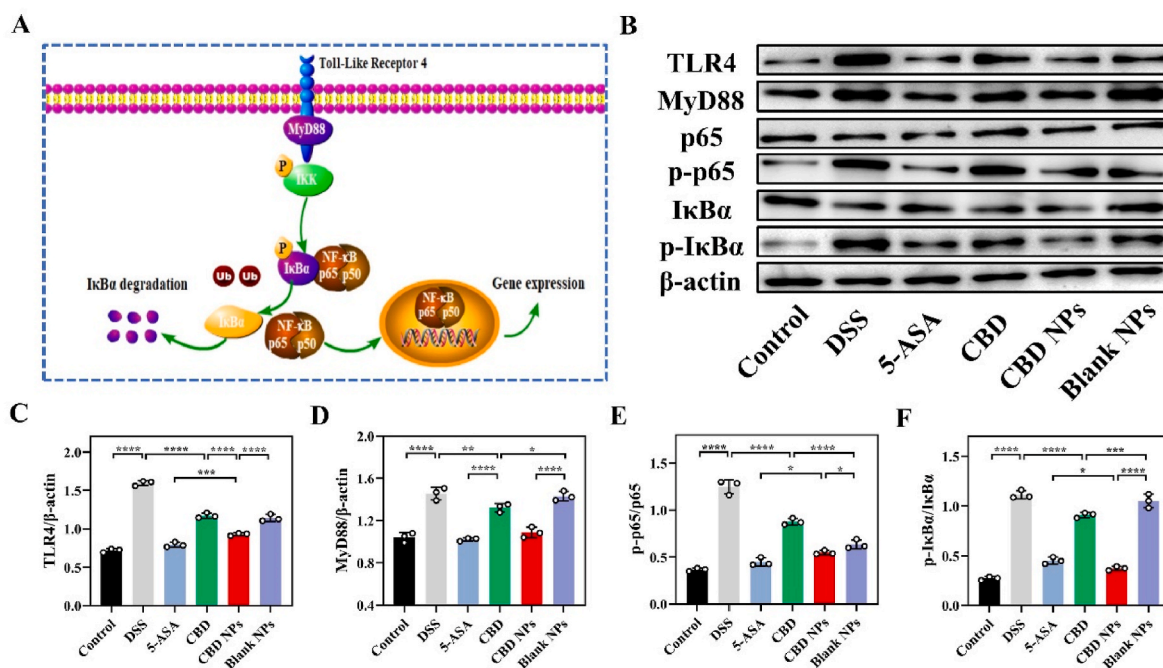
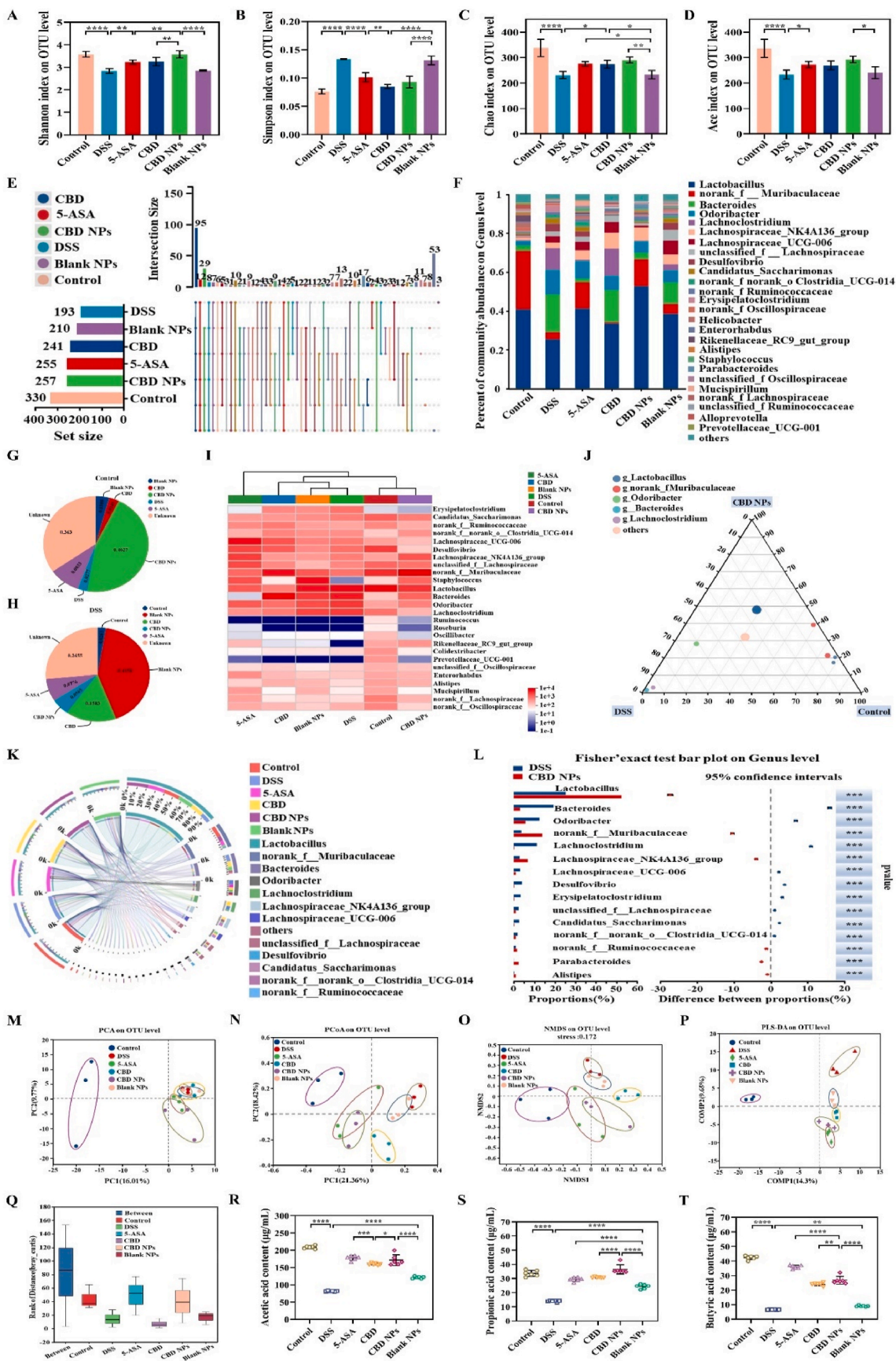


Fig. 8. Mechanisms of CBD NPs effectively alleviating UC. (A) Schematic diagram of the TLR4-NF- κ B signaling pathway. (B) Western blotting images. Protein expression levels of (C) TLR4, (D) MyD88, (E) p-p65/p65 and (F) p-I κ B α /I κ B α in colon tissues. Data are mean \pm SD (n = 3). * p < 0.05, ** p < 0.01, *** p < 0.001 and **** p < 0.0001.



(caption on next page)

Fig. 9. Effects of nanoparticles on intestinal flora of UC mice. (A) Shannon index, (B) simpson index, (C) chao index and (D) ace index based on OTU level. (E) UpSet venn diagram representing the number of common and unique species in intestinal flora of UC mice in different groups based on genus level. (F) The community composition histogram representing the intestinal flora composition of UC mice in different groups based on genus level. (G) Origin analysis of source tracker species between DSS group, 5-ASA group, CBD group, CBD NPs group, Blank NPs group and control group. (H) Source tracker species origin analysis between control group, 5-ASA group, CBD group, CBD NPs group, Blank NPs group and DSS group. (I) The community composition heatmap representing the intestinal flora composition of UC mice in different groups based on genus level. (J) Ternary phase diagram representing the composition and distribution proportion of intestinal flora of UC mice in the control group, DSS group and CBD NPs group based on species level. (K) Circos diagram representing the distribution proportion of dominant species of intestinal flora of UC mice in different groups based on genus level. (L) Significant analysis of species difference of UC mice intestinal flora in DSS group and CBD NPs group based on genus level. (M) Principal component analysis (PCA), (N) principal co-ordinates analysis (PCoA), (O) non-metric multidimensional scaling (NMDS), (P) partial least squares discriminant analysis (PLS-DA), (Q) analysis of similarities (ANOSIM) and replacement multi factor analysis of variance (Adonis) used to evaluate the similarity or difference of intestinal flora composition of UC mice in different groups based on OTU level. The content of (R) acetic acid, (S) propionic acid and (T) butyric acid in cecal contents of UC mice in different groups. Data are mean \pm SD (n = 3). * p < 0.05, ** p < 0.01, *** p < 0.001 and **** p < 0.0001.

of UC (Figs. 6 and 7), which could be attributed to the lack of circulation time and limited bioavailability of free CBD *in vivo*. Besides, the similarity of species sources between the control group and DSS group and other groups was evaluated by source tracker species source analysis. The results showed that the similarity of DSS group, 5-ASA group, CBD group, CBD NPs group and Blank NPs group with the control group was 0.0277, 0.0833, 0.0245, 0.4627 and 0.0388, respectively (Fig. 9G). It was obvious that the species origin of CBD NPs was the closest to that of the control group. On the contrary, the similarity between control group, 5-ASA group, CBD group, CBD NPs group and Blank NPs group and DSS group was 0.0263, 0.0776, 0.1583, 0.0565 and 0.4158 respectively (Fig. 9H). The species source of Blank NPs group was the most similar to that of DSS group. Next, the similarity and difference of community composition of UC mice in each group at the taxonomic level of the genus were analyzed through the community heatmap map. The results showed that the community composition of CBD NPs was the closest to that of the healthy control group (Fig. 9I), indicating that the treatment of CBD NPs had a very beneficial role in maintaining the balance of intestinal flora. Also, the composition and proportion of dominant species in all groups were reflected through Circos diagram, and the results were shown in Fig. 9K. In addition, the distribution proportions of different species in control group, DSS group and CBD NPs were measured by ternary phase diagram (Fig. 9J).

Then, the β -diversity of intestinal flora of UC mice was measured by principal component analysis (PCA analysis), principal coordinate analysis (PCoA) and non-metric multidimensional scale analysis (NMDS). The results showed that the community composition of UC mice treated with CBD NPs and 5-ASA was close to that of healthy control, which was quite different from that of UC mice in DSS group (Fig. 9M – O). This result proved that CBD NPs had excellent β diversity. Then, the significance of the difference between groups was tested by similarity analysis (ANOSIM/Adonis) and partial least square discriminant analysis (PLS-DA). The results showed that the difference between groups was significantly greater than that within groups (Fig. 9Q and P). Finally, species with different abundance in intestinal flora of UC mice in DSS group and CBD NPs group were detected to evaluate the significance of species difference between the two groups. The results showed that there were significant differences in dominant species between the two groups, such as *Lactobacillus*, *Bacteroides*, *Odoribacter*, *norank_f_Muribaculaceae*, *Lachnospiridium*, *Lachnospiraceae_NK4A136_group*, *Desulfovibrio*, etc (Fig. 9L). All the above results proved that CBD NPs could effectively maintain the homeostasis of intestinal flora by regulating the α -diversity, species composition and β -diversity of intestinal flora in UC mice induced by DSS.

3.22. Short chain fatty acid analysis

SCFAs are one of the main metabolites produced by intestinal microbiota, which play an important role in maintaining intestinal homeostasis and alleviating colitis [45]. Therefore, in this study, the content of SCFAs (acetic acid, propionic acid and butyric acid) in cecum contents of UC mice was determined by GC-MS. The results showed that the contents of acetic acid, propionic acid and butyric acid in UC mice of

DSS group decreased significantly (Fig. 9R-T). CBD NPs effectively restored the levels of acetic acid, propionic acid and butyric acid in UC mice, indicating that CBD NPs can protect the intestinal epithelial barrier and maintain intestinal homeostasis by maintaining the level of SCFAs in the intestine.

3.23. Biocompatibility of nanoparticles

First, the cytotoxicity was determined by the Calcein/PI cell activity and cytotoxicity test kit. The results showed that RAW264.7 cells showed strong green fluorescence after being treated with different concentrations of Blank NPs (Fig. 10A). After DAPI staining, the nucleus also showed a complete round shape (Fig. 10A). In addition, the results showed that the cells had high cell activity (>90 %) (Fig. 10B). The above results indicated that the nanocarriers prepared in this study had no adverse effects on cells. Next, the blood compatibility of CBD NPs was evaluated. The results showed that no hemolysis occurred within a certain concentration range after CBD NPs were incubated with plasma for 1 h or 3 h (Fig. 10C), and the hemolysis rate was below 0.1 % (Fig. 8D), which were lower than the international standard of 5 % [46, 47], indicating that CBD could maintain integrity in blood. This result was verified in the serum stability of nanoparticles. Besides, the blood biochemical indicators (WBC, RBC, PLT, Lymph, Mid, Gran, HGB, MCV, HCT, MCHC and RDW) of nanoparticles were measured. The results showed that compared with the original plasma, the hematological parameters of CBD, Blank NPs and CBD NPs remained at normal levels (Fig. S8A-L). The above results indicated that the nanoparticles prepared had excellent biocompatibility, which provided a prerequisite for the subsequent experiments.

3.24. In vivo safety of nanoparticles

Moreover, the effects of CBD, Blank NPs and CBD NPs on the liver and kidney functions of mice were evaluated. The results showed that the body weight (Fig. 10E), organ index (Fig. 10F), liver and kidney function indexes (ALT, AST, TBIL, LDH, ALB, creatinine, UA and BUN) of mice treated with the above samples had no significant difference from the control group (Fig. 10G-N). Besides, it should be noted that the heart, liver, spleen, lung, kidney and colon of the mice treated with the above samples showed no histological damage (Fig. 10O). The above results indicated that the nanoparticles prepared in this study had excellent *in vivo* safety, which provided a guarantee for their practical clinical application.

4. Conclusion

In this study, a kind of nanoparticles with redox response and dual targeting of mitochondria/colon were developed, which could be targeted to deliver CBD to the site of colitis. CBD NPs effectively alleviated the symptoms of UC mice caused by DSS, improved the level of inflammatory factors and oxidative stress, restored the intestinal mucosal barrier, and effectively maintained the homeostasis of the intestinal flora. These results indicated that the targeted nano delivery platform

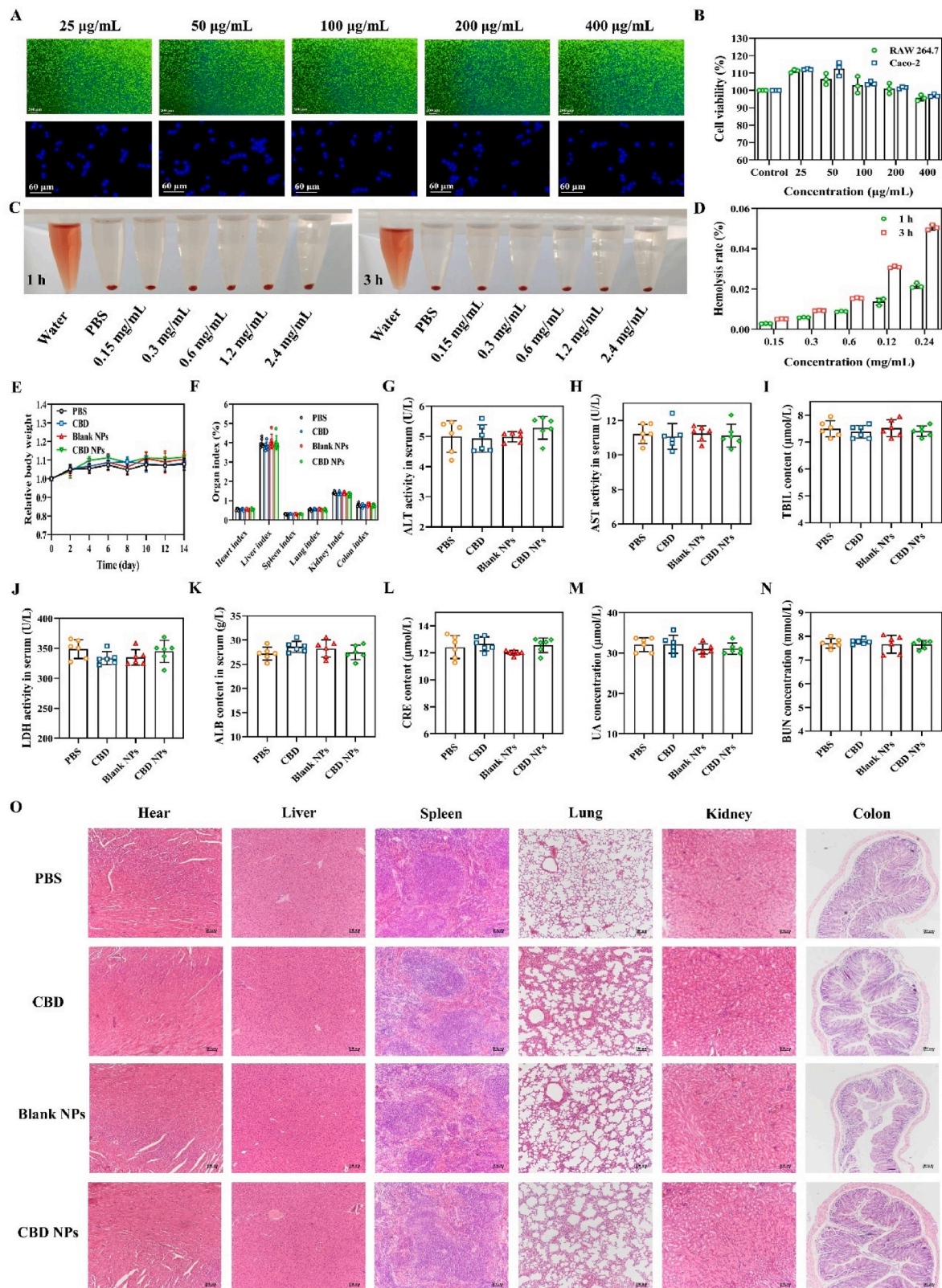


Fig. 10. Biosafety evaluation of nanoparticles. (A) Staining image of living and dead cells and nuclear image of RAW264.7 cells treated by Blank NPs for 48 h. (B) Cytotoxicity of RAW264.7 treated with Blank NPs for 48 h. Data are mean \pm SD (n = 3). (C) Hemolytic pictures and (D) hemolytic rates of CBD NPs with different concentrations incubated with plasma for 1 h or 3 h, respectively. Data are mean \pm SD (n = 3). (E) Weight of mice treated with CBD, Blank NPs and CBD NPs. (F) Organ index of mice processed by CBD, Blank NPs and CBD NPs. (G) Levels of alanine aminotransferase (ALT), (H) aspartate aminotransferase (AST), (I) total bilirubin (TBIL), (J) lactate dehydrogenase (LDH), (K) albumin (ALB), (L) creatinine, (M) uric acid (UA) and (N) urea nitrogen (BUN) in serum of mice processed by CBD, Blank NPs and CBD NPs. (O) Histological analysis of main organs in mice processed by CBD, Blank NPs and CBD NPs. Data are mean \pm SD (n = 6).

can be used as an effective tool for UC treatment.

CRedit authorship contribution statement

Xuan Zhang: Conceptualization, Data curation, Formal analysis, Investigation, Methodology, Software, Validation, Visualization, Writing – original draft, Writing – review & editing. **Xia Gao:** Formal analysis, Investigation, Validation. **Xiangzhou Yi:** Formal analysis, Validation. **Hui Yu:** Formal analysis, Validation. **Mingyang Shao:** Formal analysis, Validation. **Yongcheng Li:** Writing – review & editing. **Xuanri Shen:** Conceptualization, Funding acquisition, Project administration, Resources, Supervision, Writing – review & editing.

Declaration of competing interest

The authors declare that they have no known competing financial interests or personal relationships that could have appeared to influence the work reported in this paper.

Data availability

Data will be made available on request.

Acknowledgements

This research was supported by Scientific Research Foundation of Hainan Tropical Ocean University (grant numbers RHDRC202301).

Appendix A. Supplementary data

Supplementary data to this article can be found online at <https://doi.org/10.1016/j.mtbio.2024.100965>.

References

- J. Zhang, Y. Zhao, T. Hou, H. Zeng, D. Kalambe, B. Wang, X. Shen, Y. Huang, Macrophage-based nanotherapeutic strategies in ulcerative colitis, *J. Contr. Release* 320 (2020) 363–380, <https://doi.org/10.1016/j.jconrel.2020.01.047>.
- A. Ahmad, M.M. Ansari, R.K. Mishra, A. Kumar, A. Vyawahare, R.K. Verma, S. S. Raza, R. Khan, Enteric-Coated Gelatin nanoparticles mediated oral delivery of 5-aminosalicylic acid alleviates severity of DSS-induced ulcerative colitis, *Mater. Sci. Eng. C* 119 (2020) 111582, <https://doi.org/10.1016/j.msec.2020.111582>.
- A. Kumar, Kumar, V. Kumar, A. Ahmad, R.K. Mishra, A. Nadeem, N. Siddiqui, M. M. Ansari, S.S. Raza, K.K. Kondepudi, R. Khan, Colon-adhering delivery system with inflammation responsiveness for localized therapy of experimental colitis, *ACS Biomater. Sci. Eng.* 9 (2023) 4781–4793, <https://doi.org/10.1021/acsbomaterials.3c00480>.
- I.B.C. Lima, L.C.G.A.I. Moreno, E.C. Silva-Filho, J.M. Irache, F.J.B. Veiga, H.M. L. Rolim, L.C.C. Nunes, Development of nanostructured systems using natural polymers to optimize the treatment of inflammatory bowel diseases: a prospective study, *J. Drug Deliv. Sci. Technol.* 64 (2021) 102590, <https://doi.org/10.1016/j.jddst.2021.102590>.
- X. Feng, Q. Xie, H. Xu, T. Zhang, X. Li, Y. Tian, H. Lan, L. Kong, Z. Zhang, Yeast microcapsule mediated natural products delivery for treating ulcerative colitis through anti-inflammatory and regulation of macrophage polarization, *ACS Appl. Mater. Interfaces* 14 (2022) 31085–31098, <https://doi.org/10.1021/acscami.2c05642>.
- Y. Liu, B.G. Li, Y.H. Su, R.X. Zhao, P. Song, H. Li, X.H. Cui, H.M. Gao, R.X. Zhai, X. J. Fu, X. Ren, Potential activity of traditional Chinese medicine against ulcerative colitis: a review, *J. Ethnopharmacol.* 289 (2022) 115084, <https://doi.org/10.1016/j.jep.2022.115084>.
- V. Gowd, Kanika, C. Jori, A.A. Chaudhary, H.A. Rudayni, S. Rashid, R. Khan, Resveratrol and resveratrol nano-delivery systems in the treatment of inflammatory bowel disease, *J. Nutr. Biochem.* 109 (2022) 109101, <https://doi.org/10.1016/j.jnutbio.2022.109101>.
- A. Toscano, D.G. Ebo, K. Abbas, H. Brucker, I.I. Decuyper, D. Naimi, A. Nanda, A. P. Nayak, L.J. Skypala, G. Sussman, J.S. Zeiger, W.S. Silvers, A review of cannabis allergy in the early days of legalization, *Ann. Allergy Asthma Immunol.* 130 (2022) 288–295, <https://doi.org/10.1016/j.anaai.2022.10.016>.
- F. Majidi, F. Taheri, P. Salehi, M. Motaghinejad, S. Safari, Cannabinoids Δ^9 -Tetrahydrocannabinol and Cannabidiol may be effective against methamphetamine induced mitochondrial dysfunction and inflammation by modulation of Toll-like type-4(Toll-like 4) receptors and NF- κ B signaling, *Med. Hypotheses* 133 (2019) 109371, <https://doi.org/10.1016/j.mehy.2019.109371>.
- K. Kongkadee, W. Kongkadee, W. Wisuitiprot, K. Ingkaninan, N. Waranuch, Anti-inflammation and gingival wound healing activities of *Cannabis sativa* L. subsp. *sativa* (hemp) extract and cannabidiol: an *in vitro* study, *Arch. Oral Biol.* 140 (2022) 105464, <https://doi.org/10.1016/j.archoralbio.2022.105464>.
- C.T. Costiniuk, M.A. Jenabian, Acute inflammation and pathogenesis of SARS-CoV-2 infection: cannabidiol as a potential anti-inflammatory treatment? *Cytokine Growth Factor Rev.* 53 (2020) 63–65, <https://doi.org/10.1016/j.cytogr.2020.05.008>.
- S. Jeong, H.K. Yun, Y.A. Jeong, M.J. Jo, S.H. Kang, J.L. Kim, D.Y. Kim, S.H. Park, B. R. Kim, Y.J. Na, S.I. Lee, H.D. Kim, D.H. Kim, S.C. Oh, D.H. Lee, Cannabidiol-induced apoptosis is mediated by activation of Noxa in human colorectal cancer cells, *Cancer Lett.* 447 (2019) 12–23, <https://doi.org/10.1016/j.canlet.2019.01.011>.
- A.P. Nayak, C. Lobundo, L. Bielory, Immunomodulatory actions of cannabinoids: clinical correlates and therapeutic opportunities for allergic inflammation, *J. Allergy Clin. Immunol.* 11 (2022) 449–457, <https://doi.org/10.1016/j.jaip.2022.10.009>.
- A.A. Izzo, M. Camilleri, Cannabinoids in intestinal inflammation and cancer, *Pharmacol. Res.* 60 (2009) 117–125, <https://doi.org/10.1016/j.phrs.2009.03.008>.
- C. Wang, B. Cui, Y. Sun, C. Wang, M. Guo, Preparation, stability, antioxidative property and *in vitro* release of cannabidiol (CBD) in zein-whey protein composite nanoparticles, *LWT-Food Sci. Technol.* 162 (2022) 113466, <https://doi.org/10.1016/j.lwt.2022.113466>.
- M. Zeeshan, H. Ali, S. Khan, S.A. Khan, B. Weigmann, Advances in orally-delivered pH-sensitive nanocarrier systems; an optimistic approach for the treatment of inflammatory bowel disease, *Int. J. Pharm.* 558 (2019) 201–214, <https://doi.org/10.1016/j.ijpharm.2018.12.074>.
- X. Zhang, Y. Ma, L. Ma, M. Zu, H. Song, B. Xiao, Oral administration of chondroitin sulfate-functionalized nanoparticles for colonic macrophage-targeted drug delivery, *Carbohydr. Polym.* 223 (2019) 115126, <https://doi.org/10.1016/j.carbpol.2019.115126>.
- Y. Zhang, J. Zhang, D. Duan, The role of microbiota-mitochondria crosstalk in pathogenesis and therapy of intestinal diseases, *Pharmacol. Res.* 186 (2022) 106530, <https://doi.org/10.1016/j.phrs.2022.106530>.
- D. Wang, Y. Zhang, S. Yang, D. Zhao, M. Wang, A polysaccharide from cultured mycelium of *Hericium erinaceus* relieves ulcerative colitis by counteracting oxidative stress and improving mitochondrial function, *Int. J. Biol. Macromol.* 125 (2019) 572–579, <https://doi.org/10.1016/j.ijbiomac.2018.12.092>.
- P. Wu, S. Yao, X. Wang, L. Yang, S. Wang, W. Dai, H. Zhang, B. He, X. Wang, S. Zhang, Q. Zhang, Oral administration of nanoformulated indoximod ameliorates ulcerative colitis by promoting mitochondrial function and mucosal healing, *Int. J. Pharm.* 637 (2023) 122813, <https://doi.org/10.1016/j.ijpharm.2023.122813>.
- H. Chen, Z. Fang, M. Song, K. Liu, Mitochondrial targeted hierarchical drug delivery system based on HA-modified liposomes for cancer therapy, *Eur. J. Med. Chem.* 241 (2022) 114648, <https://doi.org/10.1016/j.ejmech.2022.114648>.
- M. Zhao, P. Li, H. Zhou, L. Hao, H. Chen, X. Zhou, pH/redox dual responsive from natural polymer-based nanoparticles for on-demand delivery of pesticides, *Chem. Eng. J.* 435 (2022) 134861, <https://doi.org/10.1016/j.cej.2022.134861>.
- Y. Dou, C. Li, L. Li, J. Guo, J. Zhang, Bioresponsive drug delivery systems for the treatment of inflammatory diseases, *J. Contr. Release* 327 (2020) 641–666, <https://doi.org/10.1016/j.jconrel.2020.09.008>.
- S.D. Wollin, P.J.H. Jones, α -Lipoic acid and cardiovascular disease, *J. Nutr.* 133 (2003) 3327–3330, <https://doi.org/10.1016/j.jconrel.2020.09.008>.
- M. He, Y. Wu, M. Hong, Z. Yun, T. Li, Y. Jiang, α -Lipoic acid treatment alleviates postharvest pericarp browning of litchi fruit by regulating antioxidant ability and energy metabolism, *Postharvest Biol. Technol.* 180 (2021) 111629, <https://doi.org/10.1016/j.jconrel.2020.09.008>.
- M. Zu, Y. Ma, B. Cannup, D. Xie, Y. Jung, J. Zhang, C. Yang, F. Gao, D. Merlin, B. Xiao, Oral delivery of natural active small molecules by polymeric nanoparticles for the treatment of inflammatory bowel diseases, *Adv. Drug Deliv. Rev.* 176 (2021) 113887, <https://doi.org/10.1016/j.addr.2021.113887>.
- W. Liu, Z. Dong, K. Liu, Y. Lu, W. Wu, J. Qi, Z. Chen, Targeting strategies of oral nano-delivery systems for treating inflammatory bowel disease, *Int. J. Pharm.* 600 (2021) 120461, <https://doi.org/10.1016/j.ijpharm.2021.120461>.
- A. Ahmad, M.M. Ansari, A. Kumar, M. Bishnoi, S.S. Raza, R. Khan, Aminocellulose-grafted polycaprolactone-coated core-shell nanoparticles alleviate the severity of ulcerative colitis: a novel adjuvant therapeutic approach, *Biomater. Sci.* 9 (2021) 5868–5883, <https://doi.org/10.1039/d1bm00877c>.
- M. Usman, C. Zhang, P.J. Patil, A. Mehmood, X. Li, M. Bilal, J. Haider, S. Ahmad, Potential applications of hydrophobically modified inulin as an active ingredient in functional foods and drugs - a review, *Carbohydr. Polym.* 252 (2021) 117176, <https://doi.org/10.1016/j.carbpol.2020.117176>.
- S. Giri, P. Dutta, T.K. Giri, Inulin-based carriers for colon drug targeting, *J. Drug Deliv. Sci. Technol.* 64 (2021) 102595, <https://doi.org/10.1016/j.jddst.2021.102595>.
- M.M. Tawfik, H. Xie, C. Zhao, P. Shao, M.A. Farag, Inulin fructans in diet: role in gut homeostasis, immunity, health outcomes and potential therapeutics, *Int. J. Biol. Macromol.* 208 (2022) 948–961, <https://doi.org/10.1016/j.ijbiomac.2022.03.218>.
- D. Wang, F. Sun, C. Lu, P. Chen, Z. Wang, Y. Qiu, H. Mu, Z. Miao, J. Duan, Inulin based glutathione-responsive delivery system for colon cancer treatment, *Int. J. Biol. Macromol.* 111 (2018) 1264–1272, <https://doi.org/10.1016/j.ijbiomac.2018.01.071>.
- L. Lian, S. Zhang, Z. Yu, H. Ge, S. Qi, X. Zhang, L. Long, X. Xiong, D. Chu, X. Ma, X. Li, H. Gao, The dietary freeze-dried fruit powder of *Actinidia arguta* ameliorates dextran sulphate sodium-induced ulcerative colitis in mice by inhibiting the

- activation of MAPKs, *Food Funct.* 10 (2019) 5768–5778, <https://doi.org/10.1039/c9fo00664h>.
- [34] R.K. Mishra, A. Ahmad, A. Kumar, A. Vyawahare, S.S. Raza, R. Khan, Lipid-based nanocarrier-mediated targeted delivery of celecoxib attenuate severity of ulcerative colitis, *Mater. Sci. Eng. C* 116 (2020) 111103, <https://doi.org/10.1016/j.msec.2020.111103>.
- [35] H. Laroui, D. Geem, B. Xiao, E. Viennois, P. Rakhya, T. Denning, D. Merlin, Targeting intestinal inflammation with CD98 siRNA/PEI-loaded nanoparticles, *Mol. Ther.* 22 (2014) 69–80, <https://doi.org/10.1038/mt.2013.214>.
- [36] H. Yang, W. Shen, W. Liu, L. Chen, P. Zhang, C. Xiao, X. Chen, PEGylated poly(α -lipoic acid) loaded with doxorubicin as a pH and reduction dual responsive nanomedicine for breast cancer therapy, *Biomacromolecules* 19 (2018) 4492–4503, <https://doi.org/10.1021/acs.biomac.8b01394>.
- [37] Z. Zhai, W. Ouyang, Y. Yao, Y. Zhang, H. Zhang, F. Xu, Dexamethasone-loaded ROS-responsive poly(thioketal) nanoparticles suppress inflammation and oxidative stress of acute lung injury, *Bioact. Mater.* 14 (2022) 430–442, <https://doi.org/10.1016/j.bioactmat.2022.01.047>.
- [38] A. Ahmad, K. Vaghasiya, A. Kumar, P. Alam, S.S. Raza, R.K. Verma, R. Khan, Enema based therapy using liposomal formulation of low molecular weight heparin for treatment of active ulcerative colitis: new adjunct therapeutic opportunity, *Mater. Sci. Eng. C* 121 (2021) 111851, <https://doi.org/10.1016/j.msec.2020.111851>.
- [39] R.K. Mishra, A. Selim, V. Gowri, A. Ahmad, A. Nadeem, N. Siddiqui, S.S. Raza, G. Jayamurugan, R. Khan, Thiol-Functionalized cellulose-grafted copper oxide nanoparticles for the therapy of experimental colitis in Swiss albino mice, *ACS Biomater. Sci. Eng.* 8 (2022) 2088–2095, <https://doi.org/10.1021/acsbomaterials.2c00124>.
- [40] W. Tian, H. Wang, Y. Zhu, Q. Wang, M. Song, Y. Cao, J. Xiao, Intervention effects of delivery vehicles on the therapeutic efficacy of 6-gingerol on colitis, *J. Contr. Release* 349 (2022) 51–66, <https://doi.org/10.1016/j.jconrel.2022.06.058>.
- [41] X. Li, S. Fang, Y. Yu, H. Yang, Y. Rao, D. Hong, C. Lu, M. Yu, X. Lu, C. Yu, Q. Zhao, Oral administration of inflammatory microenvironment-responsive carrier-free infliximab nanocomplex for the targeted treatment of inflammatory bowel disease, *Chem. Eng. J.* 445 (2022) 136438, <https://doi.org/10.1016/j.cej.2022.136438>.
- [42] Y. Chen, W. Su, S. Tie, W. Cui, X. Yu, L. Zhang, H. Hua, M. Tan, Orally deliverable sequence-targeted astaxanthin nanoparticles for colitis alleviation, *Biomaterials* 293 (2022) 121976, <https://doi.org/10.1016/j.biomaterials.2022.121976>.
- [43] M. Zu, D. Xie, B.S.B. Canup, N. Chen, Y. Wang, R. Sun, Z. Zhang, Y. Fu, F. Dai, B. Xiao, 'Green' nanotherapeutics from tea leaves for orally targeted prevention and alleviation of colon diseases, *Biomaterials* 279 (2021) 121178, <https://doi.org/10.1016/j.biomaterials.2021.121178>.
- [44] L. Li, Y. Guo, Q. Huang, X. Shi, Q. Liu, F. Wang, Q. Liu, K. Yu, Z. Wang, Anti-inflammatory properties and gut microbiota modulation of an alkali-soluble polysaccharide from purple sweet potato in DSS-induced colitis mice, *Food Sci. Hum. Wellness* 11 (2022) 795–805, <https://doi.org/10.1016/j.fshw.2022.03.010>.
- [45] H. Li, W. Cao, J. Xie, H. Che, L. Liu, X. Dong, X. Dong, L. Song, W. Xie, α -D-1,6-glucan from *Castanea mollissima* Blume alleviates dextran sulfate sodium-induced colitis *in vivo*, *Carbohydr. Polym.* 289 (2022) 119410, <https://doi.org/10.1016/j.carbpol.2022.119410>.
- [46] Y. Cui, Y. Yang, M. Ma, Y. Xu, J. Sui, H. Li, J. Liang, Y. Sun, Y. Fan, X. Zhang, Reductive responsive micelle overcoming multidrug resistance of breast cancer by co-delivery of DOX and specific antibiotic, *J. Mater. Chem. B* 7 (2019) 6075–6086.
- [47] Z. Xu, D. Yang, T. Long, L. Yuan, S. Qiu, D. Li, C. Mu, L. Ge, pH-Sensitive nanoparticles based on amphiphilic imidazole/cholesterol modified hydroxyethyl starch for tumor chemotherapy, *Carbohydr. Polym.* 277 (2022) 118827, <https://doi.org/10.1016/j.carbpol.2021.118827>.